Lepton Identification In Proton-Proton Collisions With Trilepton Final State Model Using Machine Learning

Kristoffer Langstad

Thesis submitted for the degree of
Master in Computational Science: Physics
60 credits

Department of Physics
Faculty of mathematics and natural sciences

UNIVERSITY OF OSLO

Spring 2021

Lepton Identification In Proton-Proton Collisions With Trilepton Final State Model Using Machine Learning

Kristoffer Langstad

Lepton Identification In Proton-Proton Collisions With Trilepton Final State Model Using Machine Learning

http://www.duo.uio.no/

Printed: Reprosentralen, University of Oslo

Abstract

...

Acknowledgements

...

Contents

List of Figures

Listings

Chapter 1

Introduction

In particle physics, one of the big focuses is colliding particles at nearly the speed of light using accelerators to produce other and possibly undiscovered particles. When two particles collide, they will produce new particles that move through detectors around the collision point. Since the particles are extremely small, it is not always certain that two particles may collide. That is why beams of particles are accelerated at the same time. This then produces huge amount of data each second that is captured by detectors and stored for further analysis. Many particles are produced through particle collisions, and it is not always trivial to identify all these particles. There are also cases where some particles are not detected at all, like neutrinos[1]. By using machine learning (ML) algorithms, which is a study in computer science and mathematics involving among others pattern recognition, we can try to computationally identify these newly produced particles from the collision decays.

Particle physics takes a closer look at the building blocks of the universe, the fundamental particles in the Standard Model. This is however just a theory that seems to fit well with observations. There are several observations in the universe that cannot fully be explained by the Standard Model, like dark matter and dark energy, meaning that it seems to be incomplete or have to be explained by something completely new. One of the methods to complete or expand the Standard Model is to find new particles. This is done at large complexes like CERN, where one of the things they do is to collide already existing particles to produce new particles. After colliding particles, the new particles are detected using big detectors like ATLAS. One of the major discoveries from colliding particles is the discovery of the Higgs boson[1][2], which then got added to the Standard Model. In this thesis, we

[1]Some particle physics theories are studying these undetected particles to discover their true nature.

will analyze both "*truth*"[2] and more real types of simulated data of particle collisions producing and decaying into other particles that are detected, like at the ATLAS detector at CERN.

The goal of this thesis is to use machine learning algorithms to automatically classify final state particles from many events of proton-proton collisions. We will study a few different versions of a particle physics model that gives three final state leptons and missing transverse energy (MET), and compare them with each other.

1.1 Motivation for Machine Learning

Machine learning and data science has had a huge growth in the past years. There are now a bigger variety of algorithms and approaches better suited for data analysis and different types of analyses depending on both the data sets and the desired goals. The data sets are as well a lot bigger than before, with samples ranging up to billions. This is both good and bad, since most machine learning models need a lot of training data to perform and predict on a good level. But with larger data sets, the more time is needed to do the analyses since there are more data, obviously. This means that the models have to be fast and good.

Machine learning models has pattern recognition as one of the main focuses. The idea is to automatize and learn what normally is complex and difficult for humans to do. This can include image analysis or to learn the rules of a game. The more data the learning models have, the better they can do their tasks. Even though the algorithms can do quite complex tasks, the fundamental methods in these algorithms include normally simple methods. Many of the best algorithms have several hyperparameters that are used to further train and tune the models on the data sets they are used on.

This thesis looks at the same models as Das et al. [3], with a focus on the trilepton channel, and Pascoli et al. [4] to produce the final trilepton plus missing transverse energy states. By applying machine learning techniques on simulated data that force this type of trilepton final state, we want to see if we can automatically identify the final state leptons and if we then can say something about the MET. If successful, then we can export the best model to other similar scenarios later.

[2]Meaning we have simulated data of particle collisions where we know exactly what the particles are and their origins.

1.2 Structure of Thesis

In the first chapters of part I, we take a look at an introduction to particle physics and further theories connected with the model we study. The next chapters involve the particle kinematics of particle collisions, and how they are collided together and detected by instruments, followed by a short explanation of the model to be analyzed. Then follows theory of machine learning, the learning models and evaluation metrics to be used in this thesis. The last chapter looks at the data and generation of the data prior to our analysis.

Part II consists of detailed implementation of the machine learning algorithms. The analysis is chosen to be done in the programming language **Python**, which has many useful libraries for doing machine learning.

In part III we present the results of the analysis done with the machine learning algorithms, and compare the different variations of the particle physics model we use.

Part IV consists of discussions of the results, concluding remarks of the thesis and a short look into future research based on this thesis.

Notation and Conventions

- $e = 1.6 \cdot 10^{-19}$ C : The elementary charge.
- $c = 2.998 \times 10^8$ m/s: Speed of light in vacuum.
- 1 GeV $= 10^9$ eV $= 10^9 \times 1.602 \times 10^{-19}$ J: Approximately the rest mass energy of the proton.
- $m_e = 9.109 \times 10^{-31}$ kg $= 0.511$ MeV/c^2: Mass of an electron.
- 1 barn (b) $\equiv 10^{-28}$ m^2: Interaction cross sections (dimension of area).
- $h = 6.626 \times 10^{-34}$ J·s: Planck's constant, a fundamental physical constant.
- $\hbar = \frac{h}{2\pi} = 1.055 \times 10^{-34}$ J·s: Unit of action in quantum mechanics (also called the reduced Planck constant).
- Einstein energy-momentum formula: $E^2 = p^2c^2 + m_o^2c^4$
- Coulomb force between two charged particles: $F = \frac{q_1 q_2}{4\pi\epsilon_0 r^2}$
- Natural units (from S.I. units):
  - Replace [kg, m, s] with [$\hbar$, c, GeV].
  - $\hbar c = 197$ MeV fm.
  - Use $\hbar = c = \epsilon_0 = \mu_0 = 1$.
- 1D time-dependent Schrödinger equation:

$$i\frac{\partial\psi(\mathbf{x},t)}{\partial t} = -\frac{1}{2m}\frac{\partial^2\psi(\mathbf{x},t)}{\partial x^2} + \hat{V}\psi(\mathbf{x},t)$$

- Planck scale $\sim 10^{19}$ GeV.
- GUT scale $\sim 10^{16}$ GeV.
- Magnetic fields are measured in Tesla (T).

Part I

*Theory

Chapter 2

The Standard Model of Particle Physics

Throughout the years, there have been many theories in physics of what the universe is made up of and how everything fits together. For now, the best theory/model is the Standard Model (SM) of particle physics. This theory has many times through the years proven to successfully predict and explain particles and their interactions. This model has lead to what we call elementary particles and fundamental forces, and they are the building blocks of the universe.

In this chapter we look closer at the contents of the SM involving the particles and forces, and going deeper into other underlying theories and models. Much of the information in this chapter is based upon Thomson [5] and some Elert [6].

2.1 Particle and Force Contents

The known elementary particles can be categorized into two main categories according to their spins; fermions and bosons. Fermions have half-integer spins, while bosons have integer spins. The Higgs boson is categorized as a boson but has 0 spin. In Figure 2.1 we see the categorization of the elementary particles, and the fundamental forces, in the SM. The individual categorizations will be explained in the upcoming sections. The interactions in the SM between the particles can be seen in Figure 2.2.

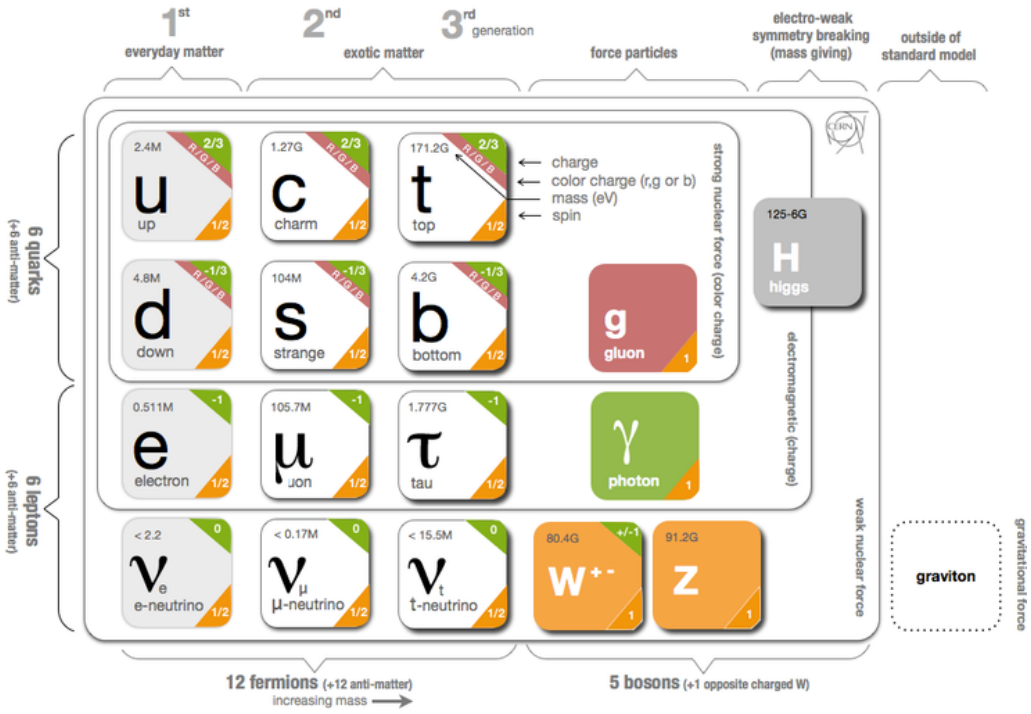

Figure 2.1: The Standard Model contents, source [7].

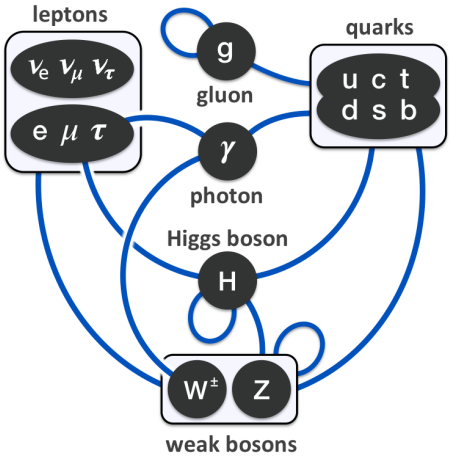

Figure 2.2: The interaction between the particles in the Standard Model. Credit: Wikipedia.

2.1.1 Gauge Bosons

From what we know of, there exists four fundamental forces. Three of these can be explained by the SM through interaction of (gauge) bosons. That is why bosons also are called force-carrier particles. The three forces are the electromagnetic, strong and weak nuclear forces, where each force has its own connected boson(s). There are five different bosons that mediates these forces, and they all have integer spins. This means that they go with vector fields, along a direction.

Strong nuclear force

The strong nuclear force is mediated by eight massless gluon (g) bosons. They only affect the (r,g,b) color charged quarks, and come in combinations of color and anti-color charges. Since the six gluons carry a different variation of color and anti-color combinations, they come in an octet of colored states. The color assignments of these eight physical gluon variations can be written as:

$$b\bar{g}, b\bar{r}, g\bar{b}, g\bar{r}, r\bar{b}, r\bar{g}, \frac{1}{\sqrt{2}}(r\bar{r} - g\bar{g}), \frac{1}{\sqrt{6}}(r\bar{r} + g\bar{g} - 2b\bar{b})$$

It is this strong interaction force that binds the quarks together to make protons and neutrons. The gluons can also self-interact with each other. This makes the interaction range of the strong nuclear force short, keeping the gluons within the nucleus. The exchange of gluons by interactions of colored particles is a mathematical model known as quantum chromodynamics (QCD, sect.2.4.2).

Electromagnetic force

The electromagnetic force is mediated by the massless photon (γ). Photons have an effect on the electrically charged particles. Since the photon is also stable and electrically neutral, it has an infinite range. The electromagnetic force is responsible for holding electrons in place around an atom, and is not as strong as the strong nuclear force. The electrically charged particles are either attracted to each other or repelled away for each other, dependent on if the charges of the particles have the same sign or not. The exchange of photons by interactions of charged particles is a mathematical model known as quantum electrodynamics (QED, sect.2.4.2).

Weak nuclear force

The weak nuclear force is mediated by the $W^{\pm}$ and Z^0 bosons. They have an affect on the flavor of the particles. There are two charge variants of the W charged boson that is either $+e$ or $-e$. The Z boson is electrically neutral. They er both massive compared to many of the other elementary particles, which gives a short lifetime and short range. Because of the difference in their charges, they act on various particles. The W boson couples the electromagnetic interactions, and also act on only left-handed particles and right-handed antiparticles. The W boson can decay to all flavors of quarks, except the top quark which is too massive, to three possible leptonic final states or hadronic final states. The Z boson interacts with left-handed particles and antiparticles. This weak interaction force can also change the flavor of quarks, and also covers isospin. The exchange of W and Z bosons by interactions with flavored particles is explained with a more complex mathematical model that unifies both the weak and electromagnetic interactions, and it is known as electroweak theory (EWT, sect.2.4.2).

Gravitational force

The last force of nature is gravity. We have not yet found the hypothetical graviton (G) particle which should carry the gravitational force. All the other forces seem to be well explained in the SM, except for gravity. So the gravitational force is not included in the SM. There has been a lot of theories about the graviton and a lot of experiments. LIGO and Virgo discovered in 2015 gravitational waves from observing the merging of two black holes with $\sim$30 solar masses each [8], which might give insight into gravitons. So far, we have nothing conclusive if the graviton exists, yet. It is thought that the graviton would have spin two, since the gravitational waves is described in general relativity as a propagating tensor disturbance. When looking at small objects (micro size), gravity does not seem to have any noticeable effect. But when we look at bigger objects of mass like humans or planets (macro size), then gravity has a much bigger effect and is well described by Einstein's General Theory of Relativity. Since gravity has more or less a negligible effect on particles, particle physicists does not have to take gravity into consideration.

2.1.2 Higgs Boson

The Higgs boson is a "recently" discovered particle (2012) [1][2] theorized by Peter Higgs in 1964. This particle has intrinsic no spin, which makes it a

scalar particle, and the only scalar particle discovered so far. Its electrically neutral, and it's massive (m_H ≈125 GeV) such that it interacts with itself. Since it is so massive, the lifetime of the Higgs boson is very short and it's hard to detect. It can in principle also decay to all SM particles, but it seems to favor the heavier particles more.

The discovery of the Higgs boson was a big contribution to the SM since it unifies and explains the masses of the other elementary particles, and why the gluons and the photon have no mass. It also confirmed the existence of the Higgs (scalar) field, which gives the other elementary particles mass when they interact with this field. This field is thought to be everywhere in the universe with a non-zero vacuum expectation value. Here, Higgs bosons appear and disappear and interact with other particles in the field giving them their masses. The gluons and photons does not interact with this field, hence they are massless.

2.1.3 Fermions

The fermion group in the SM consists of 12 elementary particles with half-integer spins. These particles are also known as matter-particles, since these particles are the building blocks of the universe. Because of their half-spins, no more than one fermion can occupy a given quantum state for a given quantum number. This is called the Pauli exclusion principle [9] which all fermions obey. Each fermion also has its own antiparticle. The antiparticles have the same mass as their particle partner, but has opposite charges and different quantum numbers. Particles that acts as their own antiparticles are called Majorana particles.

The 12 fermions can be split into two groups of six in quarks and leptons, according to how they interact from their charges. The fermions can then be related into pairs of generations, which goes from lighter and more stable to heavier and less stable. As seen in the SM figure (2.1), the first generation is called the "everyday matter". This is because most of the stable (baryonic) matter is made from the more stable first generation particles. The reason for this is that the first generation particles do not decay. second and third generation particles are more observed in high-energy environments. None of the neutrinos decay, but they rarely interact with baryonic matter.

Quarks

The six quarks are up, down, charm, strange, top and bottom. A characteristic property for the quarks is that they all have color charges and electric charges, affected by the gluons and strong nuclear force. They also carry weak

isospin The colors come in red, green and blue and the all have an anti-color. Quarks cannot come as free particles, except for the top quark which is the heaviest elementary particle. This leads to a strong binding between quarks as seen in the description of the strong nuclear force (sect.2.1.1). From this strong binding force, the quarks form particles called hadrons like protons and neutrons. They are made up of either three quarks (baryons/triplets) or a quark and an anti-quark (mesons/doublets). A proton is made up of one down quark and two up quarks. The hadrons are color-neutral particles. Since quarks have electric charges, they also interact via the electromagnetic force and the weak nuclear force.

Leptons

The six leptons are electron, electron neutrino, muon, muon neutrino, tau and tau neutrino. The electron, muon and tau leptons have electric charges and are influenced by electromagnetism. They all carry a $-1e$ electric charge, while their respective antiparticle have electric charge $+1e$. Every lepton also carry a lepton number, which is conserved in all known interactions, and a weak isospin such that they interact weakly. Both leptons and antileptons have their respective lepton number +1 and -1, and each flavor has each own lepton flavor number with the same values as the lepton numbers. There are three generations where the three electromagnetic leptons are paired with their respective neutrino, and the masses of these three leptons increases with the generation. Only the electron (1st gen) is stable and doesn't decay, while the muon and tau leptons decay via the weak interaction. The first generation can contribute to the production of stable hadrons.

2.2 Neutrinos

The three neutrinos (electron, muon, tau) are a little more special than the other elementary particles. They are classified as leptons with half-integer spins, but they do not carry any charge and are then neutral. So they only interact via the weak nuclear force, making them very hard to track since they go through almost everything even though they are stable particles. There are some theories on if the neutrinos have antiparticles[1] or if they are Majorana neutrinos. If they are Majorana, then they are the only fermions that are Majorana since all the other fermions have some electric charge. By detection of neutrinos and antineutrinos, it is only found neutrinos with left-handed chirality while antineutrinos are found with right-handed chirality.

[1]Meaning they are Dirac particles.

This comes from the weak interaction where the parity is broken. From the weak nuclear force mediator particles, the $W^{\pm}$ bosons, we know that they only couple to left-handed particles and right-handed antiparticles. This means that interaction of the right-handed neutrinos is not covered in the SM. Since mass terms couple both left- and right-handed states, the neutrinos are considered as massless in the SM. It is therefore not clear if neutrinos have a mass or not yet, but it is thought from experiments that they have a very small mass at least. Through the discovery of neutrino oscillations [10], we know that the neutrinos can change flavor given proper conditions to a different type of neutrino, meaning they cannot be massless. So, one type of neutrino can in fact change flavor to another type of neutrino when it travels over a large distance. This neutrino oscillation describes the difference of the neutrino flavor eigenstates and the neutrino mass eigenstates. This type of physics is not covered by the SM and will be looked more into later.

2.2.1 Neutrino Oscillations

From the SM we know that for all interactions the lepton number is conserved for both the total and each lepton flavor separately in beta-decay. So the lepton number is then conserved when a $W^{\pm}$ boson decays into a lepton/associated lepton neutrino pair.

The discovery of the neutrino oscillations have been done by several experiments. The two biggest contributions to the discovery of the neutrino oscillations came from the Super-Kamiokande Observatory and the Sudbury Neutrino Observatories (SNO) experiments. They got the Nobel Prize in physics in 2015 for their contributions by detecting solar neutrinos from β-decay in the Sun [11]. The Super-Kamiokande detected electron neutrinos using a big water Čerenkov detector, but they got a too low electron neutrino flux than what was expected to be produced in the Sun. The SNO experiment showed that the atmospheric neutrinos and the neutrino flux from β-decay in the Sun had strong muon and tau components by using heavy water. This meant that the solar neutrinos could be measured with different physical processes for the neutrino flavors. Since only electron neutrinos are produced by nuclear fusion in the Sun, the neutrinos have to have the ability to change their flavor when moving over large distances.

The neutrino oscillation is a quantum-mechanical phenomenon, where the neutrino flavor (weak) eigenstates (ν_e, ν_μ, ν_τ) can be related to the mass

eigenstates (ν_1, ν_2, ν_3) by an unitary transformation matrix U as

$$\begin{pmatrix} \nu_e \\ \nu_\mu \\ \nu_\tau \end{pmatrix} = \begin{pmatrix} U_{e1} & U_{e2} & U_{e3} \\ U_{\mu 1} & U_{\mu 2} & U_{\mu 3} \\ U_{\tau 1} & U_{\tau 2} & U_{\tau 3} \end{pmatrix} \begin{pmatrix} \nu_1 \\ \nu_2 \\ \nu_3 \end{pmatrix}.$$

So the flavor eigenstates are linear combinations of the mass eigenstates. The 3×3 unitary matrix is the Pontecorvo-Maki-Nakagawa-Sakata (PMNS) matrix, and it's expressed with three mixing (rotation) angles and a complex Dirac CP violation phase. The unitary of the PMNS matrix implies that $U^{-1} = U^\dagger \equiv (U^*)^T$ and $UU^\dagger = I$.

If the neutrino mass eigenstates are not the same, we get neutrino oscillations from the phase differences in components of the wavefunction. Since we already know that the neutrinos change flavor from the discovery of neutrino oscillations, we know that the neutrinos need some mass, differing by flavor, to being able to change flavor. That is why at least two of the neutrinos need non-zero masses and not the same for neutrino oscillations to be true. From experimental measurements, like long baseline accelerators, for the neutrino masses there is only found upper limits to the masses. The upper limits on the neutrino masses is found to be

$$\sum_{i=1}^{3} m_{\nu_i} \lesssim 1\text{eV}. \tag{2.1}$$

The reason why the neutrino masses seems to be so much smaller than the other fundamental particles is not known or covered by the SM to this date.

2.3 Symmetries

Particle dynamics are heavily influenced by symmetries and laws of conservation. From classical Newtonian physics, we know that energy (E), three-momentum $(\vec{p})$ and total angular momentum (J) are conserved quantities. This is also the cause in the SM. A quantity that is not conserved is the (rest) mass (m). This is something we know according to Einstein's Special Relativity. This leads to the ability to produce heavier particles in particles colliders than the particles used to collide at the start.

Another fundamental symmetry of physical laws is the CPT theorem. The CPT theorem is one of the results concluded by quantum field theory (QFT), and states that all physical processes are symmetric under CPT-transformation [12]. C is charge conjugation, where every particle can be replaced by its antiparticle. P is parity reflection, where everything in the

universe is mirrored along the three physical axes. T is time reversal, where the direction of time is reversed in the sense of looking at the local properties of the SM. The combination of these three symmetries is predicted by the SM to be a symmetry, while each symmetry alone is only a near-symmetry. The CPT symmetry gives rise to that particles and antiparticles have identical masses, magnetic moments, etc. The CPT is also thought to ba an exact symmetry in the Universe. Only the weak interactions of quarks and leptons seems to violate the C-, P-, T- and CP-symmetries out of the three fundamental forces explained by the SM.

A topic to be further discussed later is gauge theory (sect. 2.4.2). From the connected gauge symmetry in the SM, we get a conservation of certain quantum numbers during the different interactions with the fundamental forces based on the $SU(3) \times SU(2) \times U(1)$ group. The conserved quantities that are conserved are: the color charge for the strong nuclear interaction ($SU(3)$), the electric charge for electromagnetic interactions ($U(1)$) and the weak isospin for the weak nuclear interaction ($SU(2)$).

Other important conservation laws are the conservation of baryon number, B, and lepton number, L_x, in an interaction. x is the lepton flavor. The only case where the lepton number is not conserved is for neutrino oscillation. As we have explained earlier, neutrinos can change flavor when traveling large distances. But, this is not something we have to be concerned about in our case.

2.4 Quantum Field Theory

To explain the Standard Model as we know it today, we need quantum field theory (QFT). This is a theory that combines quantum mechanics, special relativity and field theory. In other words, quantum field theory tries to explain the little things in the universe, like the elementary particles, that move very fast, close to or with light speed c. This also says that every elementary particle has its own associated field. These fields can then be explained in terms of the Lagrangian density, $\mathcal{L}$, to explaining the dynamics and kinematics of the fields.

The combination of quantum mechanics and special relativity does give some problems. The most important equation in quantum mechanics is the Schrödinger equation, and it's not Lorentz invariant. The problem with this is that Schrödinger's equation is not the same for two observers in different reference frames. Other problems this leads to is that we get violation of causality, negative energy states and there is no possibility for new particle creations. The good thing is that these problems can be fixed by exchang-

ing the Schrödinger equation (see Notation and Conventions) by the Dirac equation [13][14] for $\frac{1}{2}$-spin particles and the Klein-Gordon equation [13][14] for scalar particles. With the Dirac and Klein-Gordon fields, this leads to specific (gauge) theories for different particles and associated interactions, which we have briefly mentioned earlier and will explain more soon.

2.4.1 The Lagrangian

For more simple classical mechanics cases the Lagrangian is just given as the difference between the kinetic energy and the potential energy, $L = K - V$. This is also a baseline for the QFT. By using the Lagrangian of a system with a set of generalized coordinates q_i and their time derivatives $\dot{q}_i$, we can find the equation of motion that describes the system by using the Euler-Lagrange equation,

$$\frac{d}{dt}\left(\frac{\partial L}{\partial \dot{q}_i}\right) - \frac{\partial L}{\partial q_i} = 0. \tag{2.2}$$

A difference for QFT is that instead of kinetic and potential energies, or the generalized coordinates, we use fields with four space-time coordinates. This changes the Lagrangian L to the Lagrangian density $\mathcal{L}$ as a continuous system. This is a function of the fields, $\phi_i(t, x, y, z)$, and their derivatives, $\partial_\mu \phi_i(t, x, y, z)$. Since L is the spatial integral over $\mathcal{L}$,

$$L = \int \mathcal{L} d^3\mathbf{x}, \tag{2.3}$$

and using the principle of least action [15], the new Euler-Lagrange equation becomes

$$\partial_\mu \left(\frac{\partial \mathcal{L}}{\partial(\partial_\mu \phi_i)}\right) - \frac{\partial \mathcal{L}}{\partial \phi_i} = 0. \tag{2.4}$$

For simplicity we will just call the Lagrangian density as the Lagrangian from now on. From this new Euler-Lagrange equation, we can derive both the free-particle Dirac and the Klein-Gordon equations by imposing the Lagrangian with a free fermion field[2] and free theory[3] respectively. The Lagrangian for the spin-half (spinor) field, ψ, is

$$\mathcal{L}_D = i\bar{\psi}\gamma^\mu \partial_\mu \psi - m\bar{\psi}\psi, \tag{2.5}$$

and the Lagrangian for the non-interacting scalar field, ϕ, is

$$\mathcal{L}_S = \frac{1}{2}(\partial_\mu \phi)(\partial^\mu \phi) - \frac{1}{2}m^2\phi^2. \tag{2.6}$$

[2]Relativistic spin-half fields, Chapter 17.2.2 in Thomson [5]
[3]Relativistic scalar fields, Chapter 17.2.2 in Thomson [5]

Both of these two equations for the Lagrangian contain a kinematic term and a mass term.

With perturbation theory in quantum mechanics, the Lagrangian can also be used to describe the behavior and interaction of elementary particles with Feynman diagrams for simpler visualization of usually complex particle interactions.

2.4.2 Qauge Theories

To further explain the interactions between the elementary particles, which we now know from the new Lagrangian varies depending on the particles and associated interactions, we need a new theory. In this theory we need to require that the Lagrangian stays invariant under local transformations using symmetry or gauge groups. In special relativity, this global symmetry group is called the Poincaré group which includes spacetime symmetries.

To describe the SM we need an internal gauge invariant symmetry that represents the different elementary interactions and is independent of spacetime coordinates, and this is the local $SU(3) \times SU(2) \times U(1)$ gauge symmetry group (Lie group). Here each special unitary group with degree n (the number in the parenthesis) is connected to its own gauge theory and the three elementary interactions in the SM, and n is a n-dimensional space. If a symmetry group is commutative, meaning that regardless of what the order of the elements are applied the result will be the same, then it is called an Abelian group. If the group is non-commutative, it is then a non-Abelian gauge theory which implies the existence of gauge boson self-interaction.

Quantum chromodynamics (QCD)

The gauge theory that defines the strong interaction between the quarks and (eight) gluons (color charged particles) is the quantum chromodynamics sector [16]. The QCD conserves the separately conserved color charges red, green and blue, and thus works in a three dimensional color space. Another quantity that is conserved in QCD is parity. This comes from that the QCD interaction Hamiltonian is invariant under parity transformations (sect. 11.2.2 in Thomson [5]). The antiquarks carry the opposite color charge to the quarks of red, green and blue. The color states consists of color isospin and color hypercharge. It also ensures invariance under the local gauge transformation. The gauge symmetry group for this sector is $SU(3)_C$ and is represented by 3×3 matrices, where the C stands for the conserved color. This symmetry group does not commute and is then non-Abelian gauge theory, or more precise it is a Yang-Mills gauge theory [17]. By using this gauge theory,

we can derive a new invariant Lagrangian which does not have a mass term for the gluons:

$$\mathcal{L}_{QCD} = \bar{\psi}(i\gamma^\mu \partial_\mu - m)\psi - \frac{1}{2} g_s \bar{\psi}\gamma^\mu \lambda_a \psi G^a_\mu - \frac{1}{4} G^a_{\mu\nu} G^{\mu\nu}_a \tag{2.7}$$

ψ is a fermion (quark) field, g_s is a coupling constant of the strong interaction, γ^μ are Dirac matrices, $a = 1, ..., 8$ is the eight gluons, λ_a is one of the eight Gell-Mann matrices and $G^a_{\mu\nu}$ is a gauge invariant gluon field strength tensor. This Lagrangian (eq.2.7) implies that the gluons should be massless and can self-interact.

In Figure 2.3 we see the QCD vertices for quark and gluon interactions (and self-interacting gluons) as seen by writing out the new Lagrangian (eq. 38 in Ecker [16]).

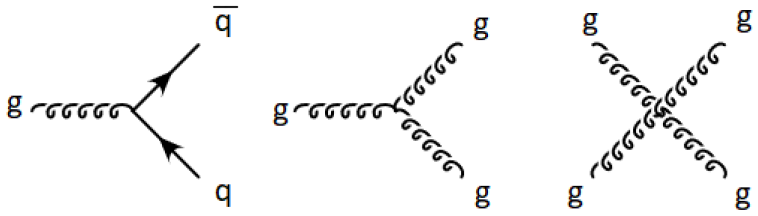

Figure 2.3: Here we see Feynman diagrams of the basic QCD vertices. From left to right we see, the coupling of gluon fields (g) interaction with quark fields (q), a triple gluon vertex and a quartic gluon vertex. Source Fig. 10.1 in Thomson [5].

Quantum electrodynamics (QED)

The gauge theory that defines the electromagnetic interaction for the electrically charged particles and photons is the quantum electrodynamics sector [18]. The QED conserves the electric charge of the particles, and the antiparticles have opposite electric charge to the particle. Like in QCD, parity is conserved in QED (sect. 11.2.2 in Thomson [5]). The gauge symmetry group for this sector is $U(1)$ and is an Abelian group. By starting with a free fermion field for the Lagrangian (eq.2.5, is invariant under *global* $U(1)$ transformation) and make it invariant under the local phase transformation. This leads to a Lagrangian with a Lorentz-invariant description where there is an electromagnetic interaction between fermions and the gauge field of the massless photon:

$$\mathcal{L}_{QED} = \bar{\psi}(i\gamma^\mu \partial_\mu - m_e)\psi + e\bar{\psi}\gamma^\mu \psi A_\mu - \frac{1}{4} F_{\mu\nu} F^{\mu\nu} \tag{2.8}$$

ψ is the field of the half-spin particles, e is a coupling constant of the electromagnetic interaction, γ^μ are Dirac matrices, A_μ is a covariant four-potential (gauge field), and $F_{\mu\nu}$ is an electromagnetic field strength tensor.

From this Lagrangian (eq.2.8) we can get the Feynman diagram of the QED interaction vertex in Figure 2.4 between a single photon and two spin-half fermions.

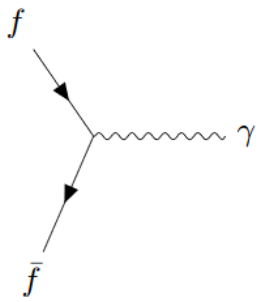

Figure 2.4: Here we see a Feynman diagram of the basic QED vertex of the interaction between fermions (f) and a massless photon (γ). Source Fig. 5.6 (and 10.10a) in Thomson [5].

Electroweak theory (EWT)

The gauge theory that defines the weak interaction for the flavor charged particles and the W and Z bosons/fields is the quantum flavordynamics (QFD) sector. Unlike QCD and QED, it is found experimentally that parity is not conserved in the weak interaction (sect. 11.2.3 in Thomson [5]). This parity-violation makes the weak interaction treat left-handed and right-handed particles differently. The charge-current weak interaction is invariant under $SU(2)$ local phase transformations and includes weak isospin.

The cross-section of W-pairs produced at higher energies, violates quantum mechanical unitarity such that particle probability is no longer conserved. At these higher energies, the electromagnetic and weak interactions become more and more similar in strength. That is why a unification of these two interactions is more used in particle physics, and it introduces the neutral Z boson as the solution to the cross-section. This unified theory is known as electroweak theory (EWT) [19] or Glashow-Weinberg-Salam (GWS) theory. This theory (from the 1960's) earned the three contributors Glashow[20], Weinberg[21] and Salam[22] the Nobel Prize in Physics in 1979 [23][24]. What makes the EWT theory more complicated than the QCD and QED theories is that the fermions exists as left- and right-handed chirality

states, while W-bosons only couple to left-handed fermions. The EWT conserves the flavor charge and weak isospin of the particles. It is this introduced weak isospin quantum number that accounts for the W-boson coupling, since left-handed fermions have half-isospin and appears as isospin doublets while right-handed fermions appear as isospin singlets. Something to take notice of here is that, the weakly interacting quarks are superpositions of the mass eigenstates while the strongly interacting quarks are mass eigenstates.

The electroweak theory is based on the $SU(2)_L \times U(1)_Y$ symmetry group, where L is left-handed interaction and Y is the weak hypercharge consisting of an electric charge Q and the third component of the weak isospin I_3, $Y = 2(Q - I_3)$. This new $U(1)_Y$ local gauge symmetry is used instead of that in QED, where the charge now has been replaced by the weak hypercharge. Each gauge invariant transformation in this theory, introduce new gauge fields which as linear combinations corresponds to the photon and W and Z bosons of the weak interaction. With these new gauge fields, we can derive yet another new preliminary (electroweak) Lagrangian that is associated with the EWT theory:

$$\begin{aligned}\mathcal{L}_{EWT} =& \bar{\psi}_L \gamma^\mu \left[i\partial_\mu - \frac{1}{2} g \boldsymbol{\sigma} \mathbf{W}_\mu - \frac{1}{2} g' Y B_\mu \right] \psi_L + \bar{\psi}_R \gamma^\mu \left[i\partial_\mu - \frac{1}{2} g' Y B_\mu \right] \psi_R \\ & - \frac{1}{4} B_{\mu\nu} B^{\mu\nu} - \frac{1}{4} \mathbf{W}_{\mu\nu} \mathbf{W}^{\mu\nu} \end{aligned} \tag{2.9}$$

$\psi_{L,R}$ are the fields for left- and right-handed fields respectively, g and g' are coupling constants related to the elementary charge, γ^μ are the Dirac matrices, $\boldsymbol{\sigma}$ are the Pauli matrices, B_μ is a field strength tensor for the weak hypercharge gauge field for $U(1)_Y$, $\mathbf{W}_{\mu\nu}$ is a field strength tensor for the three weak isospin gauge fields for $SU(2)_L$. We also have to account for the left- and right-handed states such that we don't destroy the gauge invariance, like including the fermion mass term that mixes the left- and right-handed fields. The complete EWT Lagrangian will be looked at soon.

This EWT gauge symmetry group is non-Abelian, and a Yang-Mills gauge theory. In Figure 2.5 and 2.6 we see Feynman diagrams of the electroweak interaction vertices including fermions and gauge boson self-interactions we get from the Lagrangian in equation 2.9. There we see that the photon and the Z-boson couple with both left- and right-handed fermions, while the W-bosons do not. Here we have described the interactions between the fields even though the Lagrangian (eq.2.9) does not contain any mass terms, making it not fully complete since we know that fermions have mass and that W and Z bosons are massive.

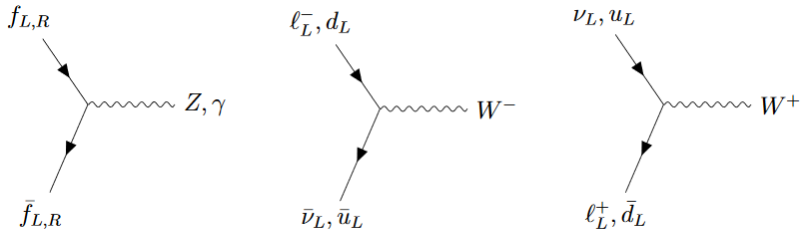

Figure 2.5: Here we see Feynman diagrams of the electroweak interaction vertices that includes fermions.

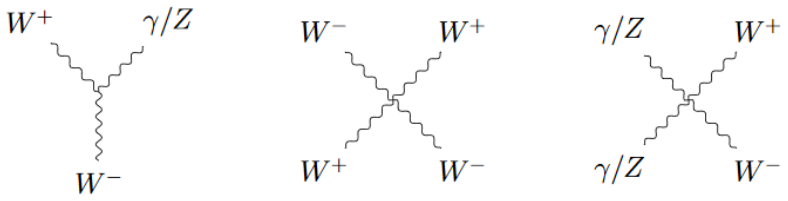

Figure 2.6: Here we see Feynman diagrams of the electroweak interaction vertices for gauge boson self-interaction.

2.4.3 Higgs Mechanism

As mentioned in the Higgs boson section 2.1.2, it is the Higgs boson that contributes to the masses of the fundamental particles in the SM that have mass, by creating the quantum scalar Higgs field in the vacuum in all of space. Leptons and bosons interact differently with the Higgs field, where the W and Z bosons acquire masses when the Higgs field has a vacuum expectation value at a critical temperature. Up till this point, the Lagrangians do not contain any mass terms yet since these terms would break up the symmetry and gauge invariance needed. With the Higgs mechanism, which is also called the Brout-Englert-Higgs (BEH) mechanism, the Higgs field is used to explain the masses of the bosons in the electroweak theory without breaking the local gauge symmetry. This concept is based on what is called spontaneous symmetry breaking.

Spontaneous symmetry breaking

In the lowest energy state of a field we find the minimum of a potential. This is also called the vacuum state. The requirements for the three gauge theories discussed is that the Lagrangian is invariant under local transformations of these theories, and that does not happen when we include the mass terms. The fermions will consistently develop mass, while the weak

interaction bosons will emerge when at lower energies.

For a **real scalar field**, there are two cases we have to consider. One is where we have $\mu^2 > 0$, where μ is the mass, which gives the vacuum expectation value to zero. Remember that the Lagrangian is kinetic terms minus potential terms, and that the vacuum expectation value is defined as the minimum of the potential. In this case we have a finite minimum. Under these circumstances, we have invariance under transformation and symmetry of the Lagrangian. In the other case when $\mu^2 < 0$, the vacuum expectation value is non-zero and the previous mass term need a new interpretation. Here we have several minima, one with + sign and one with − sign. Since we have a choice of vacuum state, this breaks the symmetry of the Lagrangian. This is spontaneous symmetry breaking. The potential and the Lagrangian are still symmetric under transformation, but because of the new interpretation of the mass term we need to rewrite the Lagrangian to a state with zero as vacuum expectation value. A new field is introduced which makes the Lagrangian no longer symmetric under field transformation, but now contains a mass term again. The Lagrangian is now expressed as the excitation of one of the minima where the field is interpreted as small perturbations about the chosen vacuum state.

For a **complex scalar field**, we consider the two same cases as above. With a complex scalar field, the Lagrangian is symmetric under global $U(1)$ transformations. For the first case ($\mu^2 > 0$) with the complex scalar field split into to real scalar fields, the symmetry of the Lagrangian is also conserved here when the two scalar fields are zero. This has an expected vacuum value of zero. For the second case ($\mu^2 < 0$), the potential gets an infinite amount of minima which forms a circle in the 2D-field plane known as the "Mexican hat"-potential. This vacuum state breaks the global $U(1)$ symmetry. With a reasonable set of variables for the vacuum state, we introduce two new fields which is used to describe the first complex scalar field. The Lagrangian now contains terms where one can be interpreted as a mass term and some as interaction terms. This Lagrangian ends up with a massive scalar field and a massless scalar field. The massless field is called a Goldstone boson, which comes from the Goldstone theorem [25] that states that a massless field will appear whenever a continuous symmetry is spontaneously broken.

The Brout-Englert-Higgs mechanism

To get to a theory with massive gauge bosons, we need to look at spontaneous symmetry breaking for local electroweak gauge theory. This theory that gives the gauge bosons mass without breaking the gauge theory is known as the Brout-Englert-Higgs mechanism. First we look at local $U(1)$ symmetry

breaking, and then we look at the complete local $SU(2)_L \times U(1)_Y$ gauge group.

Local $U(1)$ symmetry breaking: We look first at a complex scalar field ϕ with a potential and require that the Lagrangian is invariant under the local gauge transformation. This basically leads to the QED Lagrangian for a scalar field (eq.2.8), but with an extra self-coupling term. When we compare with the second case, $\mu^2 < 0$, in the spontaneous symmetry breaking, tha vacuum state is degenerate and the $U(1)$ symmetry is spontaneously broken by the vacuum state. We now introduce two new fields η and ξ used to rewrite the Lagrangian. The breaking of the symmetry has now lead to a massive scalar field η and a massless Goldstone boson ξ. The previously massless gauge field A_μ has now acquired a mass term, giving the gauge bosons of the local gauge symmetry mass.

This rewritten Lagrangian has a few problems we need to look more into. First, an extra degree of freedom seems to have been introduced by the added mass term. Second, there is a term coupling the Goldstone field ξ and the gauge field A, meaning that the spin-1 gauge field can change into a spin-0 scalar field. The solution to these problems is to use a Unitary gauge, which changes the transformations under $U(1)$. The complex scalar field is now chosen to be a real field. The Lagrangian now contains two massive fields, the (scalar) Higgs field h and the gauge field A. It also contains Higgs self-interaction terms and interaction terms between the Higgs boson and gauge boson. The Goldstone boson has now disappeared from the Lagrangian.

Local $SU(2)_L \times U(1)_Y$ symmetry breaking: For the $SU(2)_L \times (U1)_Y$ local gauge symmetry, the simplest Higgs field consists of two complex scalar fields which are placed in a weak isospin doublet. The Lagrangian with this complex scalar double contains a Higgs potential. Once again to break the symmetry in the ground state, a choice of $\mu^2 < 0$ must be taken. The Higgs doublet will now be expressed in the unitary gauge, giving a Salam-Weinberg model Lagrangian. By writing the Lagrangian to respect the $SU(2)_L \times U(1)_Y$ local gauge symmetry of the electroweak model, the mass terms can be achieved. The Lagrangian now contains three massive gauge fields for $W^\pm, Z^0$, one massless gauge field B_μ and a massive scalar field h. The massless neutral gauge boson can be identified as the photon, while the other masses are

$$m_H = \sqrt{2\lambda}v, \quad m_W = \frac{1}{2}g_W v, \quad m_Z = \frac{1}{2}v\sqrt{g_W^2 + g'^2}, \tag{2.10}$$

which depends on the vacuum expectation value of the Higgs field v (found to be 246 GeV), the coupling constant of the $SU(2)_L$ gauge interaction g_W, the coupling constant of the $U(1)_Y$ gauge interaction g'^2 and the free Higgs

potential parameter $\lambda > 0$.

The EWT theory, in addition to the coupling in Figure 2.5 and 2.6, now contains coupling between the Higgs boson and the massive gauge boson and Higgs self-interaction. These couplings can be seen in Figure 2.7.

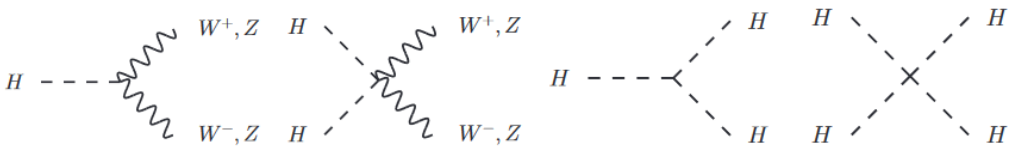

Figure 2.7: Here we see Feynman diagrams of the couplings between the Higgs boson and the massive gauge bosons and Higgs self-interaction.

Fermion masses: The Higgs mechanism can also be used to give masses to the fermions as well as the gauge bosons. The Higgs isospin doublet has a lower and an upper element. The lower element is used to give masses to down-type quarks and charged leptons, while the masses of the up-type quarks are constructed from the conjugate doublet. The gauge invariant mass terms of the Dirac fermions are then described as

$$m_f = \frac{g_f v}{\sqrt{2}}, \tag{2.11}$$

where g_f is the Yukawa coupling constant of the fermions to the Higgs field.

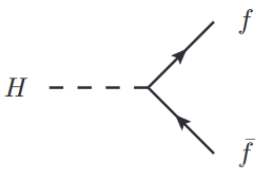

Figure 2.8: Here we see Feynman diagrams of the coupling between the Higgs boson and fermions.

Full EWT Lagrangian

With all the theory for the EWT theory we have covered, we can develop the full EWT Lagrangian:

$$\begin{aligned}\mathcal{L}_{EWT} =& \overline{\psi}_L \gamma^\mu \left[i\partial_\mu - \frac{1}{2} g \boldsymbol{\sigma} \mathbf{W}_\mu - \frac{1}{2} g' Y B_\mu \right] \psi_L + \overline{\psi}_R \gamma^\mu \left[i\partial_\mu - \frac{1}{2} g' Y B_\mu \right] \psi_R \\ & - \frac{1}{4} B_{\mu\nu} B^{\mu\nu} - \frac{1}{4} \mathbf{W}_{\mu\nu} \mathbf{W}^{\mu\nu} + \left| \left(i\partial_\mu - \frac{1}{2} g \boldsymbol{\sigma} \mathbf{W}_\mu - \frac{1}{2} g' Y B_\mu \right) \phi \right|^2 \\ & - V(\phi) - (g_f \overline{\psi}_L \phi \psi_R + G'_f \overline{\psi}_L \phi_c \psi_R + h.c.) \end{aligned} \tag{2.12}$$

The first line is the couplings between the fermions and the gauge fields and kinetic terms for the fermion fields. The second line is the kinetic terms for the gauge fields and the Higgs field, the couplings between the gauge field and the Higgs field, and the couplings between the gauge fields. The third line contains the scalar potential, the Yukawa coupling terms and the fermion mass terms, and $h.c$ stands for the corresponding Hermitian conjugate.

Chapter 3

Theories Beyond the Standard Model

The SM is just a theory that seems to explain a lot of the physics in the Universe we see from experiments, like the theory we have covered earlier with the interaction between the elementary particles and how some have mass. The SM can be seen as a model with many (25 or so) free parameters that are chosen to match our observations. But it does not explain everything, like the existence of the graviton and gravity and more. To goal for most researchers is now to try and extend the SM to a Unified field theory or a Theory of everything, that explains all the physical phenomena which the original SM does not.

One of these things is that we only seem to know what about 5% of the matter in the Universe are. This 5% of the matter in the Universe is visible to us, called baryonic matter, while the rest is something yet unknown. One theory is that the about 25% is something called dark matter, that acts as matter and has a gravitational pull in the Universe. It is thought that if dark matter is a particle and since it has a gravitational effect on baryonic matter, it must have a mass. This is seen by looking at galaxies in the Universe where the visible mass alone can't contribute to the observed velocity distributions of stars in galaxies. Since we can't seem to detect any electromagnetic radiation of dark matter, it is thought that they do not have any electric charge. So the neutrino seems like a candidate that could fit. But studies and computer simulations show that this would lead to a *hot dark matter* universe, whereas observations show that the universe must have *cold dark matter* to explain the galaxy formations. Other cosmological observations also provide evidence of this dark matter, but no concrete results of what this actually is have been presented to this date. The remaining 70% is then thought to be dark energy, which has a pushing affect on the galaxies

in the Universe making it expand faster and faster with time as it seems now. This we know even less about what could be.

When one looks closer at the SM, one can suspect that there might be some underlaying symmetry principle unifying some of the free SM parameters mentioned. The Supersymmetry theory goes beyond the SM and predicts the existence of weakly interacting massive particles (WIMPs) as an extension to the SM, which might be (cold) dark matter particles with masses in the range of a few GeV to TeV. Supersymmetry is one of the hot and bigger theories in particle physics today, where much of the focus is to observe these WIMP particles through production at the LHC (more in section 5) or as direct detection in galaxies.

We will look more into this and a few other aspects and theories about the neutrino in this chapter which the classic SM does not cover.

3.1 Supersymmetry

One of the more popular extensions to the SM is Supersymmetry (SUSY) theory, and the Minimal Supersymmetric Standard Model (MSSM) [26] with a minimal amount of new particles introduced. The foundation for this theory is that each particle in the SM has a super-symmetric partner, *sparticles*, with half a unit spin difference. The fermion superpartners are called *sfermions* and are spin-0 scalars, and similarly for the spin-1 gauge fields their superpartners are called *gauginos* with spin-half. Fermions get an "*s-*" in front of their name, while gauge fields gets an "*-ino*" ending. They are denoted with a tilde sign above their names, such that the superpartner for a W-boson is a *wino* $\tilde{W}$. These sparticles are yet to be discovered. The mass and other properties of the SM particles would have been the same for their respective superpartner if SUSY was an exact symmetry. Since these superpartners have not been discovered yet, the masses can't be the same. Meaning that SUSY must be a broken symmetry and that the sparticles must be heavier than the SM particles since they have not been discovered in experiments yet. The mass scale is theorized to $\mathcal{O}(1\text{ TeV})$.

One property of SUSY is that the bosons and fermions are related by a SUSY operator that commutes with the SM gauge transformations, and no new forces introduced. These representations of the gauge groups with their superpartners form supermultiplets. This leads to distinct superpartners for left- and right-handed fermions since they belong to different supermultiplets. SUSY particles will always be produced in paris in particle colliders to conserve a quantity called $R-parity$ [27], which we will not explore more here. One of the dark matter candidates are the lightest supersymmetric particles

(LSP) and they must be stable, and in MSSM this is the lightest neutralino as a WIMP. The LSP is a result of several decays from sparticles. SUSY particles have not been detected in particle colliders yet, since the LSPs are neutral they avoid detection. But they can be detected as missing transverse energy, since the total transverse energy must be conserved after collision.

SUSY is not a complete and simple theory for the full theory of the nature. Although, it seems that many quantum theories involving gravity might need SUSY as an ingredient to make sense. The big and exciting problem now is to detect these sparticles in experiments, thus proving the theory.

3.2 Neutrino Masses

According to the SM, neutrinos do not have mass. This happens because the SM only covers left-handed neutrinos, since the right-handed neutrinos do not involve in any of the fundamental interactions in the model and have not been observed so far. As mentioned earlier, we know from observations and experiments of neutrino oscillations that neutrinos have to have some mass to being able to change flavor when moving over large distances. This neutrino masses is something we need to look more into.

3.2.1 Dirac Neutrinos

Dirac particles are particles which can be distinctively separated from its antiparticle. The Dirac field is described by a four-component Dirac spinor ψ and can be divided into a left-handed ψ_L and a right-handed ψ_R part as two component Weyl spinors:

$$\psi = \begin{pmatrix} \psi_L \\ \psi_R \end{pmatrix}. \tag{3.1}$$

The left-handed neutrinos in the SM are then described by this left-handed Weyl field. Since the Dirac mass term require both left- and right-handed fields in the SM, there is no Dirac mass term for the neutrinos.

If we assume neutrinos as Dirac particles, the neutrino mass is added similarly to the up-type quarks as the conjugate Higgs doublet. The gauge invariant Dirac neutrino mass term after spontaneous symmetry breaking becomes

$$\mathcal{L}_D = -m_\nu(\overline{\nu_R}\nu_L + \overline{\nu_L}\nu_R), \tag{3.2}$$

with the neutrino mass still determined by the Yukawa coupling constant as

for Dirac fermions (eq. 2.11):

$$m_\nu = \frac{g_\nu v}{\sqrt{2}} \tag{3.3}$$

The neutrino masses have been found to be several orders of magnitude smaller than the charged lepton masses. This leads to a Yukawa coupling constant $g_\nu \leq 10^{-12}$ for neutrino masses that are less than 1 eV (sect. 2.2.1). It is not known why this Yukawa constant is so small, which gives reason to that there must be something else that gives the neutrinos their masses. From this the right-handed neutrino in the SM would be sterile and only interact with the Higgs boson.

3.2.2 Majorana Neutrinos

Another option for the neutrinos, is that they can be Majorana neutrinos. This means that they can be their own antiparticles. The result of this would mean that the lepton number no longer is conserved, which it is in the SM. To not break the gauge invariance of the SM when adding the fields for RH neutrinos and LH antineutrinos in the Lagrangian, the LH antineutrinos appear as the CP conjugate field of the RH neutrino[5] defined by

$$\psi_L^c = \hat{C}\hat{P}\psi = C\overline{\psi}_R^T, \tag{3.4}$$

where C is the charge conjugation matrix.

For a Majorana neutrino we have $\psi^c = \psi$, which means that the neutrino field can be expressed with a Majorana spinor

$$\psi_\nu = \begin{pmatrix} \overline{\nu_R^c} \\ \nu_R \end{pmatrix} \tag{3.5}$$

for LH and RH neutrino fields and the CP conjugate of the RH field (or the LH antineutrino) $\overline{\nu_R^c}$. The local gauge invariant Majorana neutrino mass term, with Majorana mass M, becomes

$$\mathcal{L}_M = -\frac{1}{2}M(\overline{\nu_R^c}\nu_R + \overline{\nu_R}\nu_R^c). \tag{3.6}$$

This means that the Majorana mass term is not constrained by gauge symmetry and can be arbitrary large. The global baryon number minus the lepton number $(B-L)$ symmetry of the SM would be broken if the neutrino is a Majorana neutrino. From observations of the asymmetry between matter and antimatter in the Universe, it actually looks like the baryon number is not conserved.

3.2.3 The Seesaw Mechanism

One of many theories for the light masses of the neutrinos is to add RH neutrinos that couple to the LH neutrinos. However, this would lead to a disparity problem regarding mass scale remains. To solve this, a seesaw mechanism is introduced where the observed (light Dirac) LH neutrinos couple with very heavy (sterile) Majorana RH neutrinos. This would explain the small masses of the observed SM left-handed neutrinos and the absence of observation of RH neutrinos. The problem is that the mass scale of the RH neutrinos is unknown, since the masses of the Dirac neutrinos are still uncertain. So they could be somewhere between a few keV and possibly be light dark matter particles or have more heavy masses near the unification energy (GUT scale), where the electromagnetic, weak and strong forces have equal strength.

Type-I seesaw mechanism

There are several varieties of the seesaw mechanism which extends the SM, but the simplest one is the **Type-I seesaw mechanism**[28]. This involves the mix of LH Dirac neutrinos and RH Majorana neutrinos. In this theory there is added a right-handed neutrino for each of the SM LH neutrinos, in total three added RH neutrinos. When involving neutrinos as Majorana, we get that $\overline{\nu_L}\nu_R$ is equivalent to $\overline{\nu_R^c}\nu_L^c$. The Lagrangian after the spontaneous electroweak symmetry breaking with both the Dirac and Majorana mass terms becomes:

$$\mathcal{L}_{DM} = -\frac{1}{2}\left(m_D\overline{\nu_L}\nu_R + m_D\overline{\nu_R^c}\nu_L^c + M\overline{\nu_R^c}\nu_R\right) + h.c. \tag{3.7}$$

m_D is the Dirac mass and M is the Majorana mass. This equation can also be written in terms of a 2×2 mass matrix ($\mathcal{M}$) for the neutrinos:

$$\mathcal{L}_{DM} = -\frac{1}{2}(\overline{\nu_L}\,\overline{\nu_R^c}) \begin{pmatrix} 0 & m_D \\ m_D & M \end{pmatrix} \begin{pmatrix} \nu_L^c \\ \nu_R \end{pmatrix} + h.c. \tag{3.8}$$

By looking at the eigenvalues (λ) of the mass matrix $\mathcal{M}$ we get the physical masses of the neutrinos (in this model) as (sect.17.8.1 in Thomson [5])

$$m_\pm = \lambda_\pm = \frac{M \pm M\sqrt{1 + 4m_D^2/M^2}}{2}. \tag{3.9}$$

If we assume the Majorana mass much larger than the Dirac mass, $M >> m_D$, we get a light LH neutrino state (ν) and a heavy RH neutrino state (N) with masses

$$|m_\nu| \approx \frac{m_D^2}{M} \quad \& \quad m_N \approx M. \tag{3.10}$$

The physical neutrino states are in this case

$$\nu \approx (\nu_L + \nu_R) - \frac{m_D}{M}(\nu_R + \nu_R^c) \quad \& \quad N \approx (\nu_R + \nu_R^c) + \frac{m_D}{M}(\nu_L + \nu_L^c). \quad (3.11)$$

By looking at equation 3.10, we see that the lightness of the SM neutrinos are explained when there exists much heavier right-handed neutrinos.

Inverse seesaw mechanism

The model we are studying involves a slightly different seesaw theory, namely the so-called **Inverse seesaw mechanism** [4][3]. This is a low-scale Type-I neutrino mass model and yields heavy neutrino masses and allow large Yukawa couplings. Besides the addition of right-handed neutrinos, this model also adds three singlet fermions. This then yields three light LH neutrinos and heavy pseudo-Dirac neutrinos[29][30] with small lepton number violations in the singlet mass terms. This comes from the decay of a $W_R^{\pm}$ to a pseudo-Dirac neutrino, since a neutrino coupled to a $W_R^{\pm}$ is a pseudo-Dirac fermion. It is during this process that the lepton number is approximately conserved, and accounts for missing same-sign electron events.

Our base model is the $SU(2)_L \times SU(2)_R \times U(1)_{B-L}$ left-right symmetry group (sect 3.3) which involves this inverse seesaw mechanism, and is based on the

$$SU(3)_C \times SU(2)_L \times SU(2)_R \times U(1)_{B-L} \quad (3.12)$$

gauge symmetry. The main difference from the Type-I seesaw mechanism is that instead of a heavy Majorana mass eigenstate neutrino, we have a heavy pseudo-Dirac neutrino mass eigenstate. The mass difference (mixing) between the left- and right-handed neutrinos probe small neutrino masses. This leads to Left-Right symmetric models with the same final state as for a heavy Majorana neutrino.

3.3 Left-Right Symmetry

The theory of the Left-Right Symmetric Model (LRSM)[31, 32, 33, 34, 35] was used first to explain the parity violation where there is low energy processes. By adding a RH part to the SM gauge symmetry, $SU(2)_R$, the LRSM tries to fix the parity symmetry at high energies. This is stated in Mohapatra [28]: "... weak interactions like the strong and electromagnetic ones are parity conserving at very high energies and observed maximally parity violating V-A structure of low energy weak processes is a consequence of

gauge symmetry breaking." This changes the electroweak gauge group to $SU(2)_L \times SU(2)_R \times U(1)_{B-L}$. In the SM, the electromagnetic charge goes as

$$Q_{em} = I_3{}^{1} + \frac{Y}{2}, \tag{3.13}$$

where Y is the weak hypercharge (as in sect.2.4.2). In the LRSM, the weak hypercharge factor in the electromagnetic charge is replaced with the difference between the baryon and lepton number, and a RH part of the weak isospin $I_3{}^{2}$ [28]. This changes the electromagnetic charge to

$$Q_{em} = I_{3L} + I_{3R} + \frac{B-L}{2}. \tag{3.14}$$

The left- and right-handed weak interactions of the fermion fields (**Q**uarks and **L**eptons) in the LRSM transforms as doublets

$$\mathbf{Q}_{L,R} = \begin{pmatrix} u_i \\ d_i \end{pmatrix}_{L,R} \quad \& \quad \mathbf{L}_L = \begin{pmatrix} \nu_i \\ e_i \end{pmatrix}_L, \quad \mathbf{L}_R = \begin{pmatrix} N_i \\ e_i \end{pmatrix}_R, \tag{3.15}$$

where $i = 1, 2, 3$ stands for the generation index in the SM (see Figure 2.1). We also get three gauge-singlet fermions, S_{L_i}, leading to chiral partner fields of N_{R_i}[3].

The Higgs sector in our symmetry model (eq. 3.12) has two Higgs multiplets. One is the Higgs $SU(2)_{L,R}$ multiplet $\Delta_L \times \Delta_R$. The other breaks the electroweak symmetry and is a $SU(2)_L \times SU(2)_R$ bi-doublet Φ with vacuum expectation value (VEV)

$$\langle \Phi \rangle = \begin{pmatrix} v_u & 0 \\ 0 & v_d \end{pmatrix}^{3}. \tag{3.16}$$

A $SU(3)_R$ doublet Higgs field H_R is also introduced to break down the $SU(2)_R$ symmetry, with VEV:

$$\langle H_R \rangle = \begin{pmatrix} 0 \\ v_R \end{pmatrix} \tag{3.17}$$

This breaks the left-right symmetry $SU(2)_L \times SU(2)_R \times U(1)_{B-L}$ down to the SM symmetry $SU(2)_L \times U(1)_Y$. We then get the fermion mass terms after this symmetry breaking. The VEV of H_R (eq.3.17) contributes both

[1] $I_3 = I_{3L}$. (weak isospin in the Standard Model)
[2] This means that the SM weak hypercharge factor really is $\frac{Y}{2} = I_{3R} + \frac{B-L}{2}$.
[3] $v = \sqrt{v_u^2 + v_d^2} \approxeq 174\text{GeV}$.

to the masses of heavy neutrinos and to the masses of the broken symmetry gauge bosons $W_R^{\pm}$ and Z_R[4] as:

$$m_{W_R} \approxeq \frac{g_R v_R}{\sqrt{2}} \quad \& \quad m_{Z_R} = \frac{\sqrt{g_R^2 + g_{B-L}^2}}{\sqrt{2}} v_R \tag{3.18}$$

This then leads to a weak interaction Lagrangian[3] for the $W - W_R$ mixing after the VEV of the bi-doublet Higgs field Φ has been acquired:

$$\mathcal{L}_{weak} = (W_L^- W_R^-) \begin{pmatrix} \frac{g_L^2 v^2}{2} & -\frac{g_L g_R v^2 \sin 2\beta}{2} \\ -\frac{g_L g_R v^2 \sin 2\beta}{2} & \frac{g_R^2}{2}(v_R^2 + v^2) \end{pmatrix} \begin{pmatrix} W_L^+ \\ W_R^+ \end{pmatrix} \text{[5]} \tag{3.19}$$

This Lagrangian conserves parity prior to symmetry breaking.

[4] Both the gauge bosons are massive, but the $W_R^{\pm}$ gauge bosons have a charge while the Z boson is neutral.

[5] $\tan\beta \equiv \frac{v_d}{v_u}$.

Chapter 4

Proton-Proton Collisions

The base of what we are studying in this thesis, is the proton-proton (p-p) collision in chapter 6, like at the LHC (sect.5.2). Previously we have discussed that some of the elementary particles make up what we call hadrons, which protons are. This makes proton-proton collisions somewhat complex. When two hadrons collide, it is really a subset of the hadrons that collide. This subset is called partons, and can be quarks, antiquarks or gluons. Since it is effectively the partons that collide and not the protons, the partons only carry fractions of the total momentum of the protons. We also use the center-of-mass (CM) frame of the p-p collision system and not the CM frame of the patrons that collide. This chapter explains the basics of high energy proton-proton collisions.

4.1 Particle Kinematics

To describe the kinematics of what happens in p-p collisions, we need the momentum, energy and rest mass of the particles. The Einstein energy-momentum relation in natural units becomes

$$E^2 = p^2 + m^2. \tag{4.1}$$

Since the protons will reach very high velocities when they collide, we need to include special relativity into the equations[1]:

$$E = \gamma m \quad \text{and} \quad \mathbf{p} = \boldsymbol{\beta}\gamma m \tag{4.2}$$

These equations are dependent on the Lorentz factor

$$\gamma = \frac{1}{\sqrt{1-\beta^2}} \quad \text{and} \quad \beta = \frac{v}{c}.$$

[1] In natural units.

We then introduce the momentum as a four-vector momentum

$$P^\mu = (E, \mathbf{p}) = (E, p_x, p_y, p_z).$$

The scalar product of the four-momentum is then a Lorentz-invariant quantity

$$\begin{aligned} P^2 = P^\mu P_\mu &= E^2 - \mathbf{p}^2 \\ &= \gamma^2 m^2 - \beta^2 \gamma^2 m^2 \\ &= m^2, \end{aligned} \tag{4.3}$$

since the momentum and energy are conserved separately, the four-momentum is also conserved. Be rearranging this equation, we just end up with the Einstein energy-momentum relationship in equation 4.1. This is a very useful relation with particle collisions.

4.1.1 Colliding Particles

The reference frame of choice for colliding particles, is as mentioned the CM frame of the two colliding particles. This is defined where the sum of the three-momenta $\mathbf{p}$ is zero. When two particles collide, this means that $\mathbf{p}_1 = -\mathbf{p}_2$. And when these two particles have the same rest mass $E_1 = E_2 = E$, we get

$$(P_1 + P_2)^\mu = (2E, \mathbf{0}). \tag{4.4}$$

Now we introduce what is called a Mandelstam variable, s [5], which is defined as the squared sum of the four-momenta

$$s = (P_1 + P_2)^2. \tag{4.5}$$

This we have already found out is a Lorentz-invariant quantity. We can then draw two conclusions; One, s is a Lorentz-invariant quantity as well, and two, the $\sqrt{s} = 2E$ can be interpreted as the total energy of the CM system. This is a key quantity in particle physics for particle colliders.

From equation 4.3, we got that $P^2 = m^2$. This means that we if the colliding particles were elementary particles, $\sqrt{s}$ could be interpreted as the possible energy available for heavier particle production. This would then be an upper limit for producing a heavy particle with mass M, as $M \leq \sqrt{s}$. But since protons are not elementary particles and the p-p collisions are really collisions between partons, this limit changes. We denote the momenta carried by the two partons colliding as $\mathbf{q}_1$ and $\mathbf{q}_2$. The associated four-momenta for the partons are Q_1^μ and Q_2^μ. Since we mentioned that the

partons only carry fractions of the momenta, these fractions will be defined as x_1 and x_2 for the two colliding partons. By using what is called the Drell-Yan process (explained and derived in Thomson [5]) for a quark and an antiquark, we get the fractions given as

$$x_1 = \frac{q_1}{E} \quad \text{and} \quad x_2 = \frac{q_2}{E}. \tag{4.6}$$

To get the mass M of a produced particle from the collision with the partons, we use the same limit as for an elementary particle collision and equation 4.5 for s:

$$\begin{aligned} M &\leq \sqrt{s} \\ M^2 &\leq s \\ M^2 &\leq (Q_1 + Q_2)^2 = E^2 \left[(x_1 + x_2)^2 - (x_1 - x_2)^2\right] \\ &= 4x_1 x_2 E^2 \\ &= x_1 x_2 s \end{aligned}$$

This leads to that the produced invariant mass is equal to the CM energy of the colliding partons.

The actual values of the fractions are given by their parton distribution functions (PDFs). These PDFs can be explained as the probability of a parton with a special flavor to carry the fraction x of the proton momentum when the parton participates in a hard scattering process. In hadron-hadron collisions, these scattered patrons can be observed as jets.

From this section, we can see that the event kinematics in hadron-hadron collisions have to be explained by the three independent kinematic variables, like Q^2, x_1 and x_2.

4.1.2 Products of Particle Collisions

In particle colliders, like at the LHC, the direction of the particle beams are normally defined in the z-direction which gives $\mathbf{p} = (0, 0, p)$. This plane is the longitudinal plane. The positive y-direction is defined upwards, and the positive x-direction is defined towards the center of the ring. We can then define the transverse momentum p_T perpendicular to the z-axis as

$$p_T = \sqrt{p_x^2 + p_y^2} = \sin\theta. \tag{4.7}$$

The corresponding transverse energy is given as

$$E_T = \sqrt{p_T^2 + m^2}. \tag{4.8}$$

The total momentum can then be derived as

$$p = \sqrt{p_T^2 + p_z^2}. \tag{4.9}$$

The reason for working in the transverse (xy) plane of the initial beam direction, is that the initial momentum is zero in this direction. We want to express the kinematics in spherical coordinates in terms of the polar angle θ and the azimuthal angle ϕ.

After the collisions, the parton jets will get a boost along the beam direction. That is why we introduce a *rapidity* variable y that is used to express the jet angles:

$$y = \frac{1}{2} \ln \left(\frac{E + p_z}{E - p_z} \right) \tag{4.10}$$

What is useful with this rapidity variable, is that the rapidity differences are invariant under Lorentz boosts along the beam direction. This does not apply for θ.

After what is called a hadronisation process, the invariant mass of the system of particles that forms a jet is referred to as the jet mass. If this jet mass is small compared to the jet energy, $p_z \approx E \cos\theta$. We can then rewrite the rapidity as

$$y \approx \frac{1}{2} \ln \left(\frac{1 + \cos\theta}{1 - \cos\theta} \right) = \frac{1}{2} \ln \left(\cot^2 \frac{\theta}{2} \right) = -\ln \left(\tan \frac{\theta}{2} \right) \equiv \eta \tag{4.11}$$

This new variable η is called the *pseudorapidity*. The pseudorapidity also has the following relation with the polar angle: $\eta(\theta) = -\eta(180^\circ - \theta)$. We now have the most used set of variables (p_t, ϕ, θ) for describing the kinematics of particles in a detector. In Figure 4.1 we see the illustration of the transverse and longitudinal planes. The cylindrical shape shows how particle accelerators will be situated around the collision point.

Another useful variable associated with hadron colliders, is the angular distance between two particles

$$\Delta R = \sqrt{(\Delta\eta)^2 + (\Delta\phi)^2}. \tag{4.12}$$

The angular distance defines how much two particles are moving in the same direction or as the separation in the $\phi\eta$-space, and is invariant under longitudinal boosts.

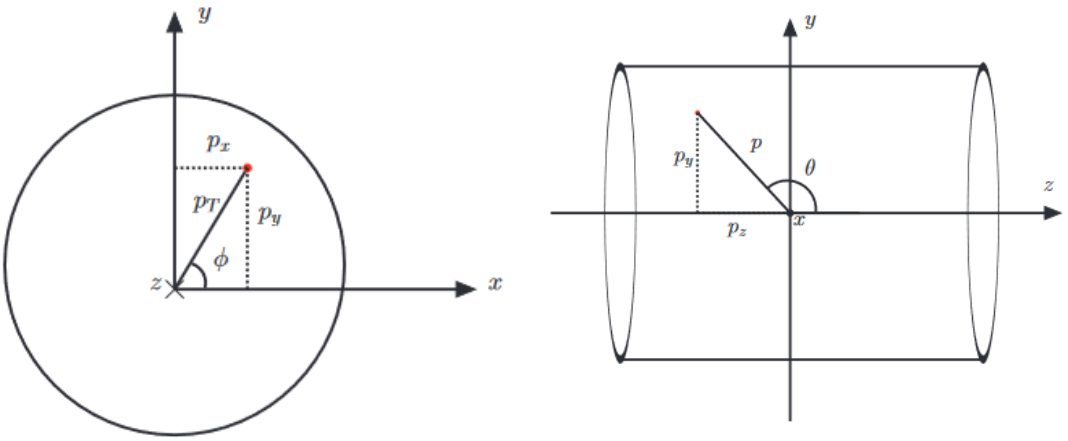

(a) The transverse plane.

(b) The longitudinal plane.

Figure 4.1: Illustrations of the (a) transverse plane and the (b) longitudinal plane. The collision point is at the origin. Figures are both from ref. [36].

4.2 Proton-Proton Interactions

When proton-proton collisions take place in colliders, the interactions can be roughly be divided into three groups:

i) elastic (el) ii) diffractive (di) iii) non-diffractive (nd)

These three groups are also components that make up the total cross-section at proton-proton colliders:

$$\sigma_{\text{total}} = \sigma_{el} + \sigma_{di} + \sigma_{nd} \tag{4.13}$$

For elastic processes, both the colliding protons remain unchanged. For the diffractive processes (di and nd), the collisions/interactions are inelastic and one or both protons will be fragmented. This leads to multi-particle final states.

The elastic and diffractive interactions have cross-sections that can not be calculated using perturbation theory, meaning they are non-perturbative processes. In these cases we get so-called *pomerons*, which are color singlet states that do not exchange color between the protons. These interaction processes at high-p_T proton-proton collisions are normally not interesting, since they will produce particles with low transverse momentum close to the beam line. They are then difficult to detect. They are still important

for luminosity measurements since they contribute to the total p-p cross-section. These events are detected in special experiments that use *minimum bias* events, where the final state has no requirements or special triggers.

4.2.1 Hard Scattering Events

The more interesting events to look at in high-p_T p-p collisions, are the non-diffraction events. With non-diffractive events, there is an exchange of color between the partons in the interaction. These are called hard scattering events. Hard scattering events with high momentum transfers, Q^2, may create heavy particles. This is the main interest in particle colliders.

A hard scattering event can be expressed as

$$A + B \to c + X, \tag{4.14}$$

where the collision between the partons are expressed as

$$a + b \to c. \tag{4.15}$$

A and B are the two colliding protons, and a and b are the corresponding colliding partons. c are the interesting high p_T objects. X are underlying products which are mostly remnants after the original collision.

In Figure 4.2 we see how a hard scattering p-p collision may look like, with outgoing partons, underlying events, initial- and final-state radiation. The initial-state radiation is mean radiation of gluons or photons from partons before the hard scattering. Final-state radiation is then the mean radiation from the produced partons after the hard interaction. The underlaying events are the further interactions between partons beyond the hard scattering. These interactions will often go out of reach of the detector. Leading to another reason for why we look at the transverse momentum.

4.2.2 Parton Distribution Function

The parton distribution function (PDF)[2] is used to describe the probability density of the two partons, a in proton A and b in proton B, to carry the proton momentum fractions x_a and x_b. These PDFs are also dependent on the squared of the momentum scale indicating the total four-momentum transfer in the collisions Q^2 as $F_{a/A}(x_a, Q^2)$ and $F_{b/B}(x_b, Q^2)$. These PDFs must be found experimentally in Deep Inelastic Scattering (DIS) experiments of leptons against hadrons, since they cannot be calculated from QCD theory. The PDFs are also used to get the cross-section of the collisions.

[2]See chapter 8 in Thomson [5] for more in depth explanations.

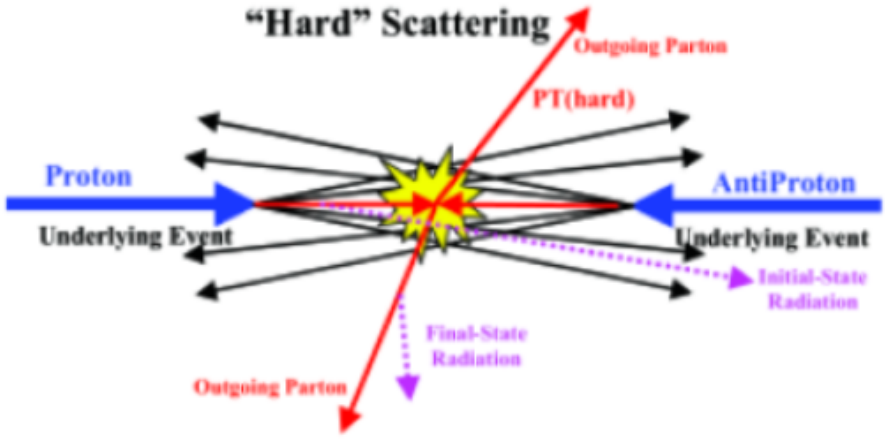

Figure 4.2: Illustration of a hard scattering proton-proton collision. Figure is taken from ref. [37].

With the measured PDFs $f(x, Q^2)$, a structure function $F_2^{ep}(x, Q^2)$ can be determined

$$F_2^{ep}(x, Q^2) = 2xF_1^{ep}(x, Q^2) = x \sum_i Q_i^2 f_i(x), \tag{4.16}$$

where i is a quark in the proton and Q_i is the charge of the quark. The interesting here are the $f(x)$ of each of the partons. So results of measurements from several DIS experiments of varying structure functions, which are superpositions of the same $f_i(x)$'s, are combined to get the $f(x)$ for each parton.

4.2.3 Hadronization

We already have covered that quarks and gluons carry color charge (sect. 2.1), and that they are not observed as free particles[3]. They can only be found in colorless objects like hadrons.

We also talked about the strong force, which increases in strength when increasing the distance between (elementary) particles. So if we separate a quark from a hadron, the color field will increase. The quarks the emits gluons, which then becomes new quark-anitquark pairs or gluons, hence making new colored particles. They will then be observed jets of colorless particles. As this production of partons continue, the energy will decrease until it is

[3]Only exception is the top quark with shorter lifetime than the QCD interaction time scale.

low enough to produce hadrons. This process of high-energy quarks (and gluons) that produce new jets until we get hadrons, is called *hadronization*. The jets can also be called hadronic showers, since many hadrons are usually produced in hadronization processes.

These jets are not only produced in p-p collisions with hard scattering, but also in the underlying events and initial- and final-state radiation gluons in this hard scattering. This makes p-p collisions very complicated and messy when trying to study them, compared to electron-positron collisions.

Chapter 5

Particle Accelerators and Collider Experiments

To fully understand the physics of the particles around us and what things are made of, we need some way of looking at the subatomic world. This is done in huge particle accelerators where particles are accelerated to high velocities and energies, and collided with each other to make other particles. Here the aftermath of the collisions result in new particles with new energies that are detected as they move through detectors.

There are various accelerators and detectors that produce and accelerate different particles in the world. In this chapter we will look at the biggest particle physics laboratory in the world, namely the European Organization for Nuclear Research (CERN[1]), and some of its components like particle accelerators, collisions and detectors.

5.1 CERN

The CERN laboratory lies near Geneva, on the border between France and Switzerland, and was founded in 1954 [38]. It is a multinational collaboration between 23 (mostly) European countries. They also have several international relations with other countries both inside and outside of Europa. CERNs main involvement today is regarding particle physics and particle accelerator experiments. Many of the biggest discoveries in particle physics today, have come from particle experiments at CERN. This includes among others, the discovery of the Higgs boson and discovery of the W and Z bosons. At the main site of CERN in Meyrin, there is also a computer facility that

[1]The name CERN is originally from French; Conseil Européen pour la Recherche Nucléaire.

is used for storing and analyzing data. These data also include simulations of particle and event experiments at CERN. CERN is also the place where Tim Berners-Lee invented the World Wide Web in the late 1980s [39].

CERN consists of several particle accelerators, experiments and facilities in different shapes and sizes. The two main types of accelerators are linear and circular. They are located at various sites, and they accelerate particles to high energies before they are sent to experiments that collides particles with other accelerated particles or particles with stationary targets, or are sent to more powerful accelerators. They are built differently to accelerate different kinds of particles with different masses. In Figure 5.1 we see the CERN accelerator complex. Some of the accelerators are mostly used to pre-accelerate the particles before they are sent to another accelerator where they are accelerated even more. This repeats until the particles reach the desired energy to collide with at one of the detectors. It normally takes about 20 minutes to reach the desired energy.

For the more important discoveries, like the ones we have mentioned above, the W and Z bosons were discovered by the Super Proton Synchrotron (SPS) in 1983. The SPS delivered an energy between 300-450 GeV. It was then later used to accelerate high energy electrons and positrons into the Large Electron-Positron Collider (LEP). LEP is the largest and most powerful lepton collider built to this date, and was most functional between 1989 and 2000. LEP was then replaced by the Large Hadron Collider (LHC) in 2008 to collide protons and heavy ions. We will look more into the LHC later (sect. 5.2).

There are also many plans for the future regarding both upgrades to existing accelerators and building new ones. The two biggest projects is the Compact Linear Collider (CLIC), which is a linear electron-positron collider at higher energies, and the Future Circular Collider (FCC), which is a even larger version of the LHC. This does not only apply at CERN, but several other places in the world like in China (CEPC [41] [42]) and Japan (ILC [43][44]).

5.1.1 Accelerators

As mentioned, there are two main types of accelerators. That is linear and circular accelerators. The first particle accelerators used static high voltage to accelerate charged particles. These accelerators are most suited for lower energies in the MV range depending on the machine. The two main types are the Cockcroft-Walton accelerator and the Van de Graaff accelerator, and they are both linear accelerators.

The more commonly used today is electrodynamic acceleration to give the

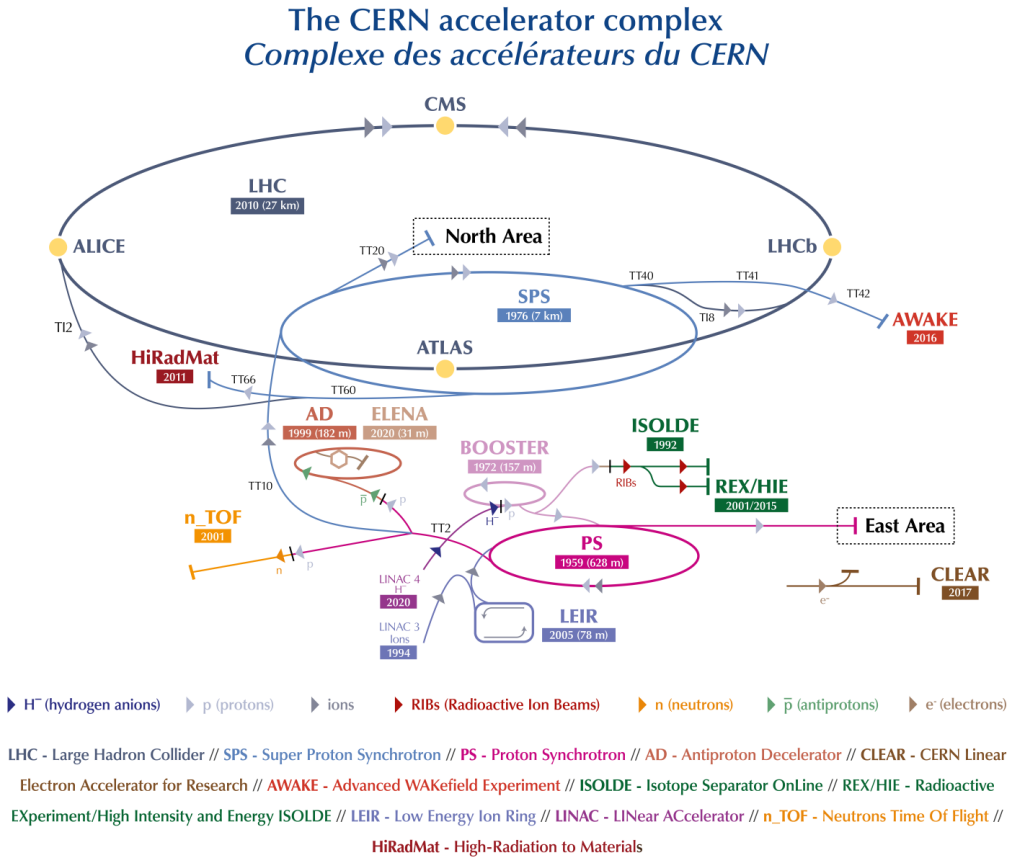

Figure 5.1: The CERN accelerator complex as of 2019. Credit: CERN[40].

particles more energy, either by non-resonant magnetic induction/resonant circuits or cavities filled with oscillating radio frequency (RF) fields. These accelerators give the particles much higher energies than the electrostatic, because of the high voltage ceiling from electric discharge when using the electrostatic.

Linear accelerators

The linear accelerators (linac) consist of several drift tubes that accelerate the particles that passes through them. The drift tubes uses an alternating high-energy field that switch between attracting the particles and then pushing them with increased velocity on the other side. These particles can reach velocities near the speed of light, depending on their initial masses. Most of the linacs are more effective for accelerating electrons and positrons since their masses are so low. The linacs are also very useful for a quick raise in the energy of the particles before injecting them into circular accelerators.

There are also linear induction accelerators that uses increasing magnetic fields due to magnetic induction to accelerate particles. This happens in non-resonant induction cavities that uses a voltage pulse to increase the magnetic field. These accelerators can reach very high beam currents in short pulses.

Circular accelerators

To reach very high beam energies in linacs, they have to be very long. This is not as big of a problem with circular accelerators. With circular accelerators, the particles just move in circles and continue to accelerate until they reach the desired energy for the experiment. This makes the space needed with higher power not as big as for the same power with a linac. To bend the path of the particle beams, electromagnets are used. The disadvantage is that every charged particle emits electromagnetic radiation when accelerated. And when a charged particle is bent around in a circle with magnets, it will emit what is called synchrotron radiation tangent to the circle. The amount of synchrotron radiation that is emitted depends heavily on the masses of the particles.

There are several types of circular accelerators with various differences. One type is the **cyclotron**, which uses a constant uniform magnetic field in a circle with the form of two D-cavities placed opposite of each other, forming a circle construction with an electric field in the gap between. There the accelerated particle moves further and further outwards as the velocity increases from the electric field. To reach higher energies than 15 MeV, the frequency of the electric charge is adjusted to the applied voltage. Now the previously

continuous beam is bunched up instead. This accelerator is called the **synchrocyclotron**. This gave a low beam intensity and needed a huge magnet radius for high energies. Next step was to keep the frequency constant and increase the magnetic field. This was the **isochronous cyclotron**, which could have continuous beams with higher intensity. This also needed bigger structures and magnets. To reach even higher energies, the **synchrotron** was introduced. This structure uses a constant radius ring where the magnetic field increases as the particles are accelerated. They need particle beam bunches to be accelerated in cavities cyclically, and uses many hundreds of bending magnets with various functions along the ring.

Some also uses what is called **storage rings**, which is a ring with many magnets with a constant magnetic field where the particle bunches continue their orbit for longer periods of time for closer study or further acceleration.

5.1.2 Colliders

As with the particle accelerators, colliders may be linear or circular. After the particle beams have been accelerated, they are either collided with other particle beams or shot against stationary targets. When the particle beams hit stationary targets, the built up energies is effectively wasted and they simply move the particles in the target. When the beams collide with each other with enough energy, they may produce new particles that often quickly decay into other particles again. These products are what scientists want to study with detectors to get more insight into physics. With colliding particles, the collision energies of the beams that can be reached are much higher than hitting stationary targets since both beams will add to the total energy when colliding. Since the particles are very small, beams at the collision points have to be extremely accurate to being able to hit the desired targets. Storage rings are quite useful for particle collisions when the particle bunches have reached their desired energies. Since the particles might miss each other on the first go, since they are so small, they can go around the ring until they finally collide without loosing to much energy.

5.2 The LHC and Accelerator Experiments

The largest and most powerful (circular/synchrotron) particle accelerator and collider today is the Large Hadron Collider (LHC) [45], which we easily can see in Figure 5.1 as the biggest gray circle around the North Area. The particles are sent in bunches up to 10^{11} particles and are accelerated mostly using radio frequency cavities in a 27 km ring consisting of superconducting

magnets, where the particles are boosted in several structures along the ring to the desired energies. The LHC is designed to have 2808 bunches at the same time traveling in the ring. The ring lies 100 m underground in a tunnel beneath the French-Swiss border. Along the ring, there are 4 main crossing points (ATLAS, CMS, ALICE, LHCb) which are detectors that register the particle collisions and the following particle decays. At these collision points, the total collision energy, or center-of-mass energy $\sqrt{s}$, can reach 13 TeV[2]. There are in total seven detectors along the ring, each designed for different experiments.

The first time, run 1, it was used for proton-proton (hadron) collisions in 2010, it reached a record high energy of 3.5 TeV per beam. After upgrades, run 2, it reached an even higher energy of 6.5 TeV per beam. It is currently stopped for another upgrade, which started in 2008. The accelerator sends two high-energy beams, in separate tubes and directions, near the speed of light before they collide at one of the detectors. To reach these high energies, the particle beams are accelerated in several systems that boosts the energies higher and higher before injected into the main LHC ring [46]. Inside the tubes, there is an ultrahigh vacuum. To make sure that the particles are directed correctly through the ring, superconducting electromagnets are used to bend the particle trajectories and keep them inside the ring. The magnets vary in strengths and sizes to direct the beams properly. Since the particles are incredibly tiny, the precision of the magnets have to be extremely good to make the particles hit each other at the collision points. That is also why beams are accelerated and not single particles at a time, and since the construction of the accelerator is a ring they can continue around again when some of them do not collide (remember storage rings sect.5.1.1). A beam can typically go around in the ring for about 10 hours before the beam has lost too much intensity.

As mentioned earlier, there are seven detector experiments at the LHC [47]. The four main, and biggest, detectors in the LHC, have different objectives. The ATLAS and CMS experiments are two large and similar general-purpose particle detectors that looks for new physics and more precise study of the Higgs boson. The ALICE and LHCb experiments have more specific roles, and study the quark-gluon plasma from heavy ion collisions and missing antimatter connected to CP-violation after the Big Bang, respectively. The remaining detectors are much smaller and are used in more specialized research. We will look more at ATLAS and the detector equipment later (sect.5.4).

The LHC is used to explore many different open questions in physics,

[2]The LHC is theorized to a limit of 14 TeV.

like further study of the SM and theories beyond it. In addition to proton-proton collisions, the LHC can also study heavy ion collisions at some of the detectors.

5.2.1 Important Parameters

One of the most important parameters of measurements at particle accelerators, are the CM energy $\sqrt{s}$ we already have mentioned. For two particles colliding, the Lorentz invariant quantity s (the squared invariant mass) is formed as

$$s = \left(\sum_{i=1}^{2} E_i\right)^2 - \left(\sum_{i=1}^{2} \mathbf{p}_i\right)^2. \tag{5.1}$$

There are also other important parameters used to describe the performance of particle colliders:

Luminosity

The second most important parameter in particle collider performance is the *luminosity*, $\mathcal{L}$. The design luminosity of the LHC is $\mathcal{L} = 10^{34}$ cm^{-2}s^{-1}. The bunches at the LHC are separated by 25 ns, which corresponds to a frequency of $f = 40$ MHz. The (instantaneous) luminosity is used to describe the number of collisions per area per second as[3]

$$\mathcal{L} = f\frac{n_1 n_2}{4\pi\sigma_x\sigma_y}, \tag{5.2}$$

where f is the frequency of the particle beam bunches colliding (bunch crossing rate), n_1 and n_2 are the number of particles in the colliding bunches and σ_x and σ_y are the root-mean-square (rms) horizontal and vertical beam sizes.

The complete collider luminosity at the LHC can be written in terms of colliding beam parameters [48]

$$\mathcal{L} = f\frac{n_1 n_2 n_b}{4\pi\sigma_x\sigma_y}F(\sigma_x, \sigma_y, \sigma_s, \Phi). \tag{5.3}$$

This equation has the same parameters as in equation 5.2, except for two additional parameters. n_b is the number of proton bunches. F is a geometrical reduction factor accounting for the non-zero-crossing angle at the interaction point, depending on the two rms beam sizes, the beam length σ_s and the crossing angle Φ.

[3] With the assumption of Gaussian profile beams and head-on collisions.

Rate

After calculating the cross-section, σ, of a collision process, the (event) *rate*, R, after accumulating many such collisions, is calculated as

$$R = \sigma \mathcal{L}. \tag{5.4}$$

Number of interactions

The total number of expected events of particles collisions over a given time, is the time integration of the event rate

$$N = \sigma \int \mathcal{L} dt. \tag{5.5}$$

The time-integral of the luminosity, $\int \mathcal{L} dt$, is often called the *integrated luminosity*, and is given in inverse femtobarns $[fb^{-1}]$.

Cross-section

Precise measurements of properties like transverse profiles are hard to get exact. This means that the instantaneous luminosity is difficult to measure accurately. Cross-section measurements are then made with reference to a process with already known cross-section, σ_{ref}. The measured cross-section is then calculated as

$$\sigma = \sigma_{\text{ref}} \frac{N}{N_{\text{ref}}}, \tag{5.6}$$

where N is the counted number of interesting events and N_{ref} is the number of observed events for the reference process.

The cross-section for p-p collisions at the LHC for $\sqrt{s} = 13$ TeV measured by the ATLAS experiment to be $\sigma \approx 78$ mb [49].

Pile-up

In particle collisions, we want a high instantaneous luminosity. This means that the intensity of the proton beam need to be high. But with high intensity proton beams, the probability of having more than one proton undergoing an inelastic interaction per bunch crossing is increased. This leads to what is called *pile-up* events, where there are several collisions from the same bunch crossing. This means we need very accurate measurements in detection of the particle tracks to distinguish which new particles comes from which collisions. The main event that is normally used in detection, and this corresponding vertex is called the *primary vertex*.

So since we want higher and higher luminosity to get more collisions, we also get more pile-ups. This need to be controlled to being able to use the data we get from the detectors of the collisions. The additional collisions do luckily normally have very small momentum transfers, which means we can characterize them as minimum bias events.

5.3 Interactions of Particles with Matter

To detect the particles produced in particle colliders like the SM, the particles have to interact with matter in the detectors. The particles also need to be stable and live long enough to be detected. Only the electron, proton, photon and neutrinos are considered stable of the known elementary particles. The unstable particles doe not decay until they have traveled a distance of order $\gamma v \tau$, where γ is the already known Lorentz factor (relativistic time dilatation) and τ is the mean lifetime of the particle in its rest frame. When the relativistic particle lifetimes are longer than 10^{-10}s, they will normally live long enough to be detected. Heavier particles has generally a shorter lifetime than lighter particles.

The particle interactions can be categorized into three categorizes: i) interactions between charged particles, ii) electromagnetic interactions between electrons and photons and iii) strong interactions of charged and neutral hadrons.

This section is based upon chapter 1.2 in Thomson [5].

5.3.1 Charged Particles

Ionization

Every electrically charged particle will interact electromagnetically. A relativistic charged particle will interact with the atomic electrons and lose energy through ionization of the atoms when it passes through a medium. This energy loss per unit length traversed through the medium by a single charged particle with velocity $v = \beta c$ is given by the Bethe-Bloch equation

$$\frac{dE}{dx} \approx -4\pi\hbar^2 c^2 \alpha^2 \frac{nZ}{m_e v^2} \left[\ln\left(\frac{2\beta^2\gamma^2 c^2 m_e}{I_e} \right) - \beta^2 \right], \tag{5.7}$$

where α is a fine-structure constant, Z is the atomic number of the medium, n is the number density of the atoms in the medium and $I_3 \sim 10Z$ eV is the effective ionization of the material averaged over all atomic electrons. From this Bethe-Bloch equation, we see that it is largest when the velocity is low.

For particle colliders, we are more interested in highly relativistic particles, $v \approx c$. In this case, dE/dx will depend logarithmically on $\beta^2\gamma^2$, where

$$\beta\gamma = \frac{v/c}{\sqrt{1-(v/c)^2}} = \frac{p}{mc} \tag{5.8}$$

makes the rate of ionization energy loss slowly rise as this factor (and p) increases. The ionization energy loss when considering the material, does not depend significantly on the material except for the material density ρ.

The energy loss due to this ionization is small, making particles where ionization is the main mechanism of energy loss able to travel long distances before their energy is completely lost. The importance of ionization differs for different type of particles. The track of ionized atoms behind charged particles that traverse through media, is used to track the trajectory of the particles.

5.3.2 Electrons and Photons

Bremsstrahlung

Another way for charged particles to lose energy, is when the energies become higher than a certain "critical energy"

$$E_c \sim \frac{800}{Z}\text{MeV} \tag{5.9}$$

related to the charge Z of the nucleus. Then the electrons will radiate a photon in the electrostatic field of a nucleus. This process of energy loss is called bremsstrahlung. For lower energies, ionization will dominate the energy loss. This process can happen for all charged particles, since the rate is proportional to the square of the mass of the particle. So as long as the energy of the particle becomes high enough, the bremsstrahlung process will have a bigger and bigger effect on the energy loss rate. This is most interesting with electrons since they get energies in the several GeV order ranges in particle experiments, way above the critical energy yielding primarily rate of energy loss due to bremsstrahlung. The typical order of the critical energy of electrons are in the order of a few tens of MeV. In lead, the critical energy for electrons are approximately $E_c \sim 10$ MeV.

The average distance over which the energy of an electron is reduced by bremsstrahlung by a factor of $1/e$, is called the *radiation length* X_0, and is dependent on the classical radius of an electron

$$r_e = \frac{e^2}{4\pi\epsilon_0 m_e c^2} = 2.8 \times 10^{-15} \text{ m}. \tag{5.10}$$

Photoelectric effect

Photons will primarily interact with materials by the photoelectric effect at low energies. The photon is then absorbed by an atomic electron which is ejected from the atom.

When the energy is around $E_\gamma \sim 1$ MeV, the Compton scattering process will dominate the process. When the photon interacts with an atomic electron here, the photon will be inelastically scattered and lose some of its energy to the electron.

At higher energies around $E_\gamma > 100$ MeV, the electron-positron pair production will dominate the process through photon interaction with the electromagnetic field of the atomic nucleus.

Electromagnetic shower

When the energy of the an electron is high enough that it radiates a bremsstrahlung photon when it interacts with a medium, the photon will produce a e^+e^- (electron-positron) pair. These new photons, electrons and positrons continue to interact with the medium and continue to produce new particles. This process is called an electromagnetic shower. This also happens when the energy of a photon is high enough.

The number of particles in an electromagnetic shower approximately doubles after every radiation length of material traversed. An illustration of an electromagnetic shower starting with an electron can be seen in Figure 5.2. The average energy of individual particles after x radiation lengths of an electromagnetic shower produced by an electron or photon is

$$\langle E \rangle \approx \frac{E}{2^x}. \tag{5.11}$$

The shower will continue to develop until the average energy goes below the critical energy E_c (eq. 5.9). From then on, the energy loss of the electrons and photons comes from ionization. There is then a maximum number of particles after x_{max} radiation lengths, at $\langle E \rangle = E_c$. The maximum radiation length is then

$$r_{max} = \frac{\ln(E/E_c)}{\ln 2}. \tag{5.12}$$

Electromagnetic showers will deposit most of their energy in a relatively small region of space. Most electromagnetic showers will also have more or less the same energy, since they will have a large number of particles leading to small fluctuations of different electromagnetic showers.

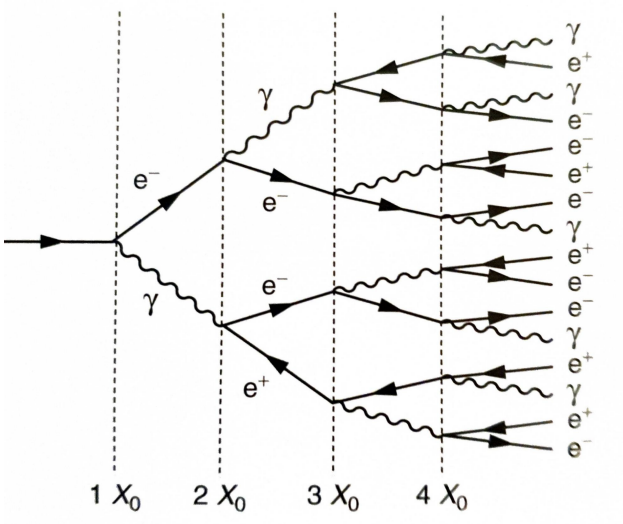

Figure 5.2: Illustration of an electromagnetic shower, beginning with an electron. Credit: ref. [5].

5.3.3 Hadrons

Like charged leptons, charged hadrons will lose energy by ionization as they traverse matter. Charged and neutral hadrons can also interact through the strong interaction by emission of a quark-antiquark pair. These types of hadronic interactions will make the hadrons split and make new hadrons and jets, leading to hadronic showers similar to electromagnetic showers. As we know, hadrons producing jets makes the hadronic shower less uinform than the electromagnetic shower. This comes from that hadronic showers can create more different final-state particles through the strong interaction than electromagnetic showers. The hadronic showers are parametrized by the mean distance between hadronic interactions of relativistic hadrons, which is called the nuclear interaction length λ_I. The nuclear interaction length is analogous to the radiation length, but it is much larger.

The hadronic showers can also get an electromagnetic component from the decay of a neutral pion (π^0) produced in the shower, since it decays almost instantaneously as $\pi^0 \rightarrow \gamma\gamma$. The fraction of electromagnetic components depends on how many neutral pions are produced in the hadronic showers. Not all of the energy in a hadronic shower many not be detected. Only on average 30% of incident energy is lost from nuclear excitation and break-up.

5.4 The ATLAS Experiment and Particle Detection

To detect the particles produced at particle colliders, we need different instruments that can detect the various types of particle interactions we have looked at in the last section. The largest detector at the LHC is the ATLAS (A Toroidal LHC ApparatuS) experiment. The ATLAS detector is 25 m in diameter, 46 m long and weights about 7000 tons. The cylindrical shape of ATLAS is optimized to detect as many particles as possible, and covers almost a 4π angle with detectors. Like we mentioned earlier for particle collisions in the LHC, the ATLAS also uses the same Cartesian coordinate system with the z-direction as the direction of the beams, y-direction is upwards and x-direction is towards the center of the accelerator circle. It also uses a spherical coordinate system with the azimuthal angle ϕ in the xy-plane around the beam axis, and the polar angle θ is the angle from the beam axis. To measure the distance between the particles, the angular distance ΔR (eq.4.12) in the $\phi\eta$-plane.

The detector can be divided into three parts; the central part is defined where the pseudo-rapidity is $|\eta| \lesssim 2.0$ and is called the *barrel*, and the two end parts ($|\eta| \gtrsim 2.0$) are called *end-caps*. In Figure 5.3 we see a computer generated image of the ATLAS detector with pointers to the main components.

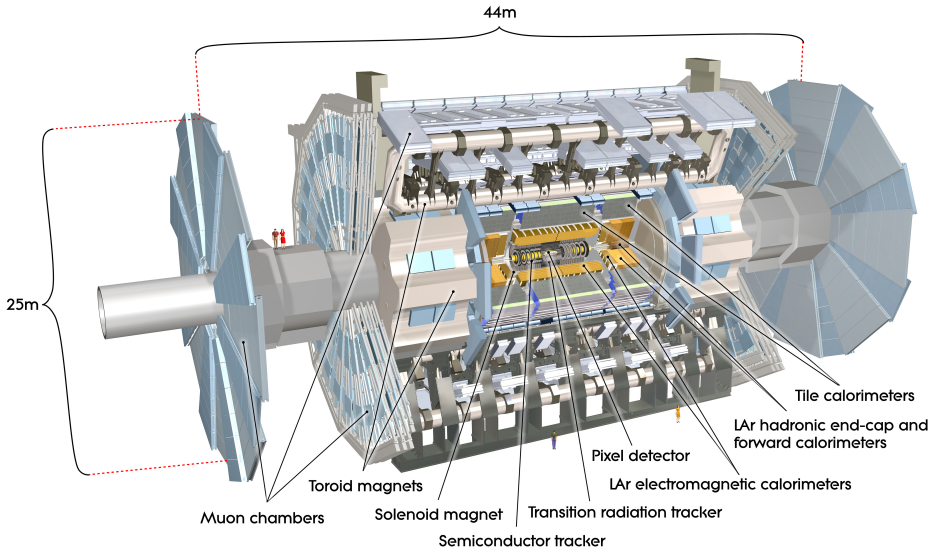

Figure 5.3: The ATLAS detector. Credit: ref. [50].

The SM detectors is designed to be a general-purpose detector, covering a wide range of signals. Some of the many particle properties the SM detector can detect is the mass, momentum and energies of the particles. For SM to detect these properties, it has a layered design of detectors that is designed to observe specific properties of the particles. These detectors use the various particle traces to identify and measure the properties of the particles. The SM detector consists of five main systems; the inner detector (ID), different calorimeters, a muon spectrometer (MS), a magnet system and a trigger and data system. The main systems also consists of smaller sub-systems, which we will take a brief look at next. In Figure 5.4, we see a sketch of the detector layout systems and how some particles behave in these different tracking systems.

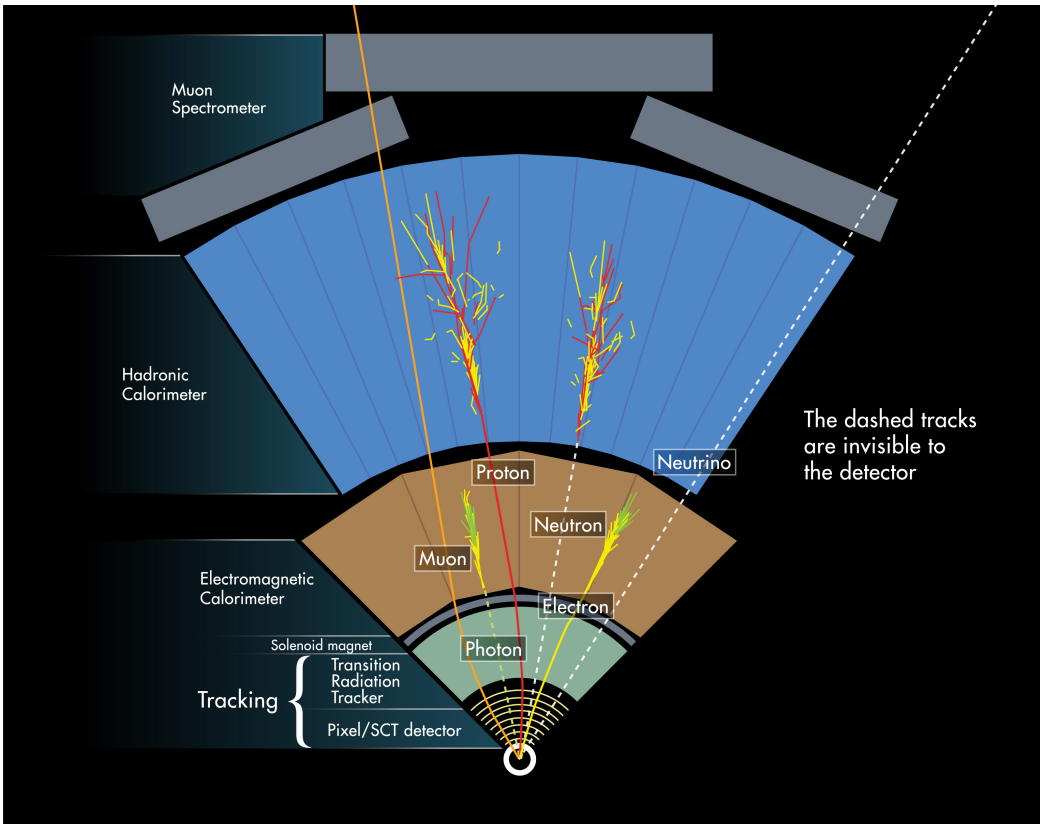

Figure 5.4: An illustration of the main tracking systems in the ATLAS detector, including how some particles behave in the various systems. Credit: ref. [51].

5.4.1 Inner Detector

The inner detector tracks charged particles that leaves traces of ionized atoms when traveling through a medium. The tracks, momentums and charges of the particles can be traced in a 2 T magnetic field that makes the charged particles curve. The degree of the curvature is used to determined the charge and the momentum.

The inner detector consists of three sub-systems. The most inner part is a silicon Pixel Detector that is used for extremely precise tracking near the interaction point of the particle collisions, which covers $|\eta| < 2.5$. The second part is a Semiconductor Tracker (SCT) that covers a bigger area than the pixel detector for the particle tracking and uses longer and narrow strips instead of pixels. The SCT provides detection in the range of $|\eta| < 2.5$ as well. The third part is a Transition Radiation Tracker (TRT) that covers an even larger area with lower spatial resolution, and can detect transition radiation photons by using gas filled drift/straw tubes. The TRT provides the capability of electron identification for a variety of energies since the transition radiation gives out a stronger signal than ionization signal. It has a coverage of $|\eta| < 2$.

5.4.2 Calorimeters

Outside the ID and the solenoid magnet system, there follows two types of calorimeters; an inner electromagnetic calorimeter and an outer hadronic calorimeter. Their purpose is to measure the energy of the passing particles and particle showers especially. They both consist of a barrel part and two end-cap parts.

The **electromagnetic** calorimeter (ECal) measures particles that interact electromagnetically like charged particles and photons. The ECal is made of layers of lead absorbing plates and liquid argon, and covers the whole ϕ angle around the beam axis. The energy is measured in the liquid argon, and free electrons are picked up by electrodes. The ECal is covered by cryostats to keep it at the correct low temperature. The thickness of the ECal is measured in radiation lengths X_0, which is the mean length required to reduce the energy of a particle by $1/E$ in a material. The thickness of the barrel part is $\geq 22X_0$, while the end-caps are $\geq 24X_0$.

The **hadronic** calorimeter (HCal) measures hadrons and hadronic showers[14]. The HCal is made of several layers of steel absorbers and plastic scintillator tiles that alternates. The HCal is a lot bigger than the ECal, since the

[14]It measures the energy of particles that interact via the strong force, which is mainly hadrons.

distance between nuclear interactions are relatively large. The HCal consists of three parts where two of them share some of the same parts as the ECal. The iron in the detector both slows down and traps hadrons and functions as a bending magnet used to reveal the charge and identity of the particles. The HCal is not as precise as the HCal. The thickness of the HCal is measured in interaction lengths λ, which is the mean distance a particle travels before interacting strongly with the material. The detector is 9.7 interaction lengths thick [52].

5.4.3 Muon Spectrometer

Outside the calorimeters, we find the muon spectrometer. Here high-energy muons are detected. Only the neutrinos should now go undetected through the detectors, in principle, and they are normally identified as missing momentum or MET. This comes from the energy conservation law, where the sum of the measured momenta of the all particles produced should be zero. This detector is very large, 11 m radius [53], and consist of three parts as well as a barrel and two end-caps; a magnetic field with three toroidal magnets, a set of 1200 chambers which measure the tracks of the muons and a set of triggering chambers with accurate time-resolution. The detection of the muons happen the same way as before, by measuring their momentum as they are bent in the detector. They should also be simpler to identify since all other identifiable particles should not reach this far out from the interaction point.

5.4.4 Magnet System

ATLAS uses two types of superconducting magnet systems to measure the momentum from the bending of the particles through the Lorentz force. The magnet system consists of a central solenoid, a barrel toroid and two end-cap toroids. The central solenoid is located between the inner detector and the electromagnetic calorimeter, which produces the 2 T magnetic field for the ID. The barrel toroid produces a magnetic field of 0.5 T, and is located around the middle cylinder of the MS barrel outside the calorimeters. The two end-cap toroids produce magnetic fields of 1 T, and located at the end-cap regions of the Muon System.

5.4.5 Trigger System

The detector produces a huge amount of data, which need to be stored and processed. The output event storage rate have to be reduced from an initial

bunch crossing of 40 MHz to ∼200 Hz . To only get the most interesting data for further analysis, a trigger system is used to extract these relevant events. The ATLAS Trigger and Data Acquisition system (TDAQ) has three levels for reducing the amount of stored data [54]; the Level 1 (LVL1) trigger is hardware-based and makes quick decisions of which events to store, the Level 2 (LVL2) and the Event filters (EF) are software-based and are often combined to and referred to as the High Level Triggers (HLT). Only the events passing both the LVL1 and HLT are stored for further analysis.

The LVL1 trigger uses information from the calorimeters and the muon spectrometer to choose the events with high p_T particles, large MET (E_T^{miss}) events and large total transverse energy E_T events. These events are then classified as interesting as passed on to the next trigger. The LVL1 trigger also defines regions based on the ϕ and η coordinates from the interesting events.

The LVL2 trigger uses all the information within the regions of interest (ROIs) defined by the LVL1 trigger to further reduce the amount of event data. The accepted events are then assembled put together into a full event. The EF uses an offline analysis to even further reduce the data used to store and further analysis at the CERN Computer Center.

Chapter 6

The Charge Current Drell-Yan Process

The model in this thesis is based on the works of Das et al. [3], Pascoli et al. [4] and CMS Collaboration et al. [55] with a $SU(2)_L \times SU(2)_R \times U(1)_{B-L}$ gauge theory combined with the inverse seesaw mechanism. Here, two protons are accelerated and collided to produce a heavy $W_R^{\pm}$ boson and a left-right symmetric model. Since the inverse seesaw mechanism allows a large left-right neutrino mixing, while keeping the neutrino masses tiny, the W_R boson may decay into a charged lepton l and a heavy pseudo-Dirac neutrino N. The pseudo-Dirac neutrino then decays into another lepton and another W_R boson with opposite sign, which then decays into another lepton and MET/a (light) neutrino:

$$q\overline{q} \to W_R \to l_1 N_l \to l_1 l_2 W_R^* \to l_1 l_2 l_3 \nu$$

The final state is then three charged leptons (trilepton) plus missing transverse energy which goes undetected as a neutrino in a detector (like ATLAS). This decay process can be seen in Figure 6.1, and is produced through the charged current Drell-Yan (CCDY) process [4].

The decay products of such particle collisions can be detected in experiments like the LHC and ATLAS (sect. 5.4). These events can also be simulated, meaning that we can simulate proton-proton collision events and the decay processes. For each decay final state product, we can measure many properties like momentum, the transverse momentum, the polar angle and the azimuthal angle. We can also detect what kind of quarks that collide[1], and which final state particles are produced. With these particle properties we can calculate the angles and angular distances between each produced

[1]Remember that we effectively collide the quarks in the protons.

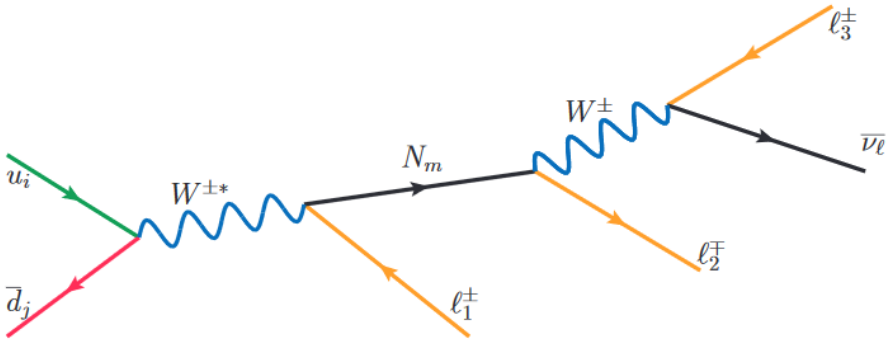

Figure 6.1: The Born diagram for the charged current Drell-Yan process of the proton-proton collision producing a heavy pseudo-Dirac neutrino N in the inverse seesaw mechanism model, leading to a trilepton plus missing transverse energy (a light neutrino) final state. Figure is taken from ref. [4].

particle and the neutrino (MET). We can also calculate the invariant masses of pairs of combined final state particles. We should then be able to find out which lepton comes from which decay branch in the decay process in Figure 6.1 computationally.

The end goal is then to make a program that can automatically identify each lepton, and where it came from, by utilizing these particle properties and using machine learning. We will look more into machine learning in the next chapters. The computational setup and input parameters for the CCDY process are look more into in a later chapter as well.

Chapter 7

Machine Learning

7.1 Introduction

Machine learning (ML) and data science are more and more used to study algorithms and statistical models. The meaning of machine learning is to use computational algorithms to automatically determine an outcome from specific patterns in data by using various algorithms that are dependent on some input and hyperparameters. With these inputs and hyperparameters, the algorithms try to learn a general pattern in often large amounts of data to find a solution. ML goes in under what is called artificial intelligence, which is where the computer takes its own decisions to produce and predict solutions to problems.

The machine learning algorithms build a model based on some given data and general rules. The data may often need to be processed in some way, like when there are missing values in the data set. The models are then fit and trained on sample data, which is a subset of the full data set. The remaining data, which is a smaller part than the training data, are used to make predictions and do an evaluation of the trained model. There is a huge variety of different evaluation metrics that are then used to check the performance of the algorithms on the data. When we have a good enough trained model, we can save it and use it later on similar data to do the same tasks on unseen data.

There is a plethora of usages for machine learning, and it is often divided into estimation or prediction problems. An example of a machine learning problem can be to identify objects in images of animals, which may be easy to humans. Algorithms can be trained to identify various animals by the algorithms given some features to best distinguish the animals from each other. This may be the shape of ears or the tail of the animals. Computationally

this means we choose some observable quantity $\mathbf{x}$ in the data we look at which are related to some parameter θ. The model $p(\mathbf{x}|\theta)$ is describing the probability of observing $\mathbf{x}$ given θ. A data set $\mathbf{X}$, also called a design matrix, is produced to fit the model. The design matrix only consists of feature data, while the class variables are stored in a target vector $\mathbf{y}$. These two datasets are often split into training and test sets, and sometimes even into training, test and validation sets. The fitting of the model then tries to find the parameters $\hat{\theta}$ which explains the data the best. In this thesis, it is the accuracy of the model that we want to optimize and focus on. Optimizing the accuracy of $\hat{\theta}$ is often the concern with estimation problems, where as prediction problems focuses more on the how the model makes new predictions. It is not always that the algorithms can give a very good prediction to all problems, or not at all in some cases depending on the datasets.

Most machine learning problems consists of the same ingredients, starting with a data set $\mathcal{D} = (\mathbf{X}, \mathbf{y})$, where $\mathbf{X}$ is the matrix containing the independent variables $\mathbf{x}$ and $\mathbf{y}$ is a vector containing the dependent variables. Then there is a model as a function $\mathbf{f} : \mathbf{x} \to \mathbf{y}$ with the parameters θ. The function is used to predict the outputs given vectors of input variables. For the predictions to take place, we need a cost function $\mathcal{C}(\mathbf{y}, \mathbf{f}(\mathbf{X}; \theta))$ that judges how well the model performs on the observations. When fitting the model, we want the $\hat{\theta}$ that explains the data the best. When considering a linear regression case with the sum of least squares as the cost function,

$$\mathcal{C}(\mathbf{y}, f(\mathbf{X}; \theta)) = \sum_{i}^{N} (y_i - f(\mathbf{x}_i; \theta))^2, \tag{7.1}$$

we get the best fit with the set of parameters that minimize the cost function:

$$\hat{\theta} = \underset{\theta}{\operatorname{argmin}} \ \{\mathcal{C}(\mathbf{y}, f(\mathbf{X}; \theta))\} \tag{7.2}$$

The ML approaches are usually divided into supervised, unsupervised and reinforcement learning [1]. **Supervised learning** already has the answers or outputs before we do anything to the model. The data set needs to be labeled and have the answers to the problem such that the algorithms know what is correct. During training, the algorithm predicts the answers from what it has learned. If we are not satisfied with the accuracy the algorithm provides, we change the hyperparameters or the algorithm until we are satisfied with the results. **Unsupervised learning** does not have any labeled data or

[1] There exists other approaches that goes beyond these three mentioned approaches. The most dominant approach today of these is called deep learning. See Goodfellow et al. [56] for more on deep learning and other possible machine learning tasks.

correct answers, meaning that it has to find its own structure in the inputs. The algorithms can only use predefined metrics to make a conclusion. This can then be used to discover hidden data patterns or to reproduce the given input. **Reinforcement learning** uses a dynamic environment that has a specific goal. As the problem is solved through trial, error and experience, the program tries to maximize its rewards from feedback during the problem solving. The program then trains itself to make decisions.

This chapter takes a closer look at the supervised learning category in machine learning and some of the basics of statistical learning, as well as we take a closer study at classification and multiclass classification, which is what is used in this thesis. The theory is mostly based on the works of Hastie et al. [57] and Mehta et al. [58].

7.2 Supervised Learning

For supervised learning, we already mentioned that we need the outputs, labeled data and the need to tune hyperparameters for optimization. The inputs may also be called independent variables, while the outputs can be called dependent variables. Supervised learning can be divided into different learning algorithms; classification, regression and active learning. **Active learning** algorithms uses a source with information to label data points with some desired output. **Regression** algorithms uses a given set of features and inputs, and estimates the relationship between the features and an outcome variable. Regression is mostly used for problems with a variation of outcome values, or a continuous output, within a range of values. **Classification** algorithms has a limited set of values as outputs, which can be categories, numbers or names. Classification uses pattern recognition in sets of categories of discrete variables to identify new observations or to group unseen data based on the inputs. We will take a closer look into the basics of statistical learning with a focus on supervised learning next.

7.2.1 Basics of Statistical Learning

In statistical learning, the goal is to find a function h in a hypothetical set $\mathcal{H}$ such that $h \in \mathcal{H}$ approximates an unknown function $y = f(x)$ as best as possible. $\mathcal{H}$ consists here of all possible functions that are defined in the domain of f and are of interest for the problem at hand. With the newly developed function $h(x)$, we would then get $h \approx f$. The *expected error* for a particular function h over all inputs x and outputs y is given by the cost

function $\mathcal{C}$ and the joint probability distribution for x and y as:

$$\mathbb{E}[h] = \int_{X\times Y} \mathcal{C}(h(x), y)\rho(x, y)dxdy. \tag{7.3}$$

In this case we need knowledge of the probability distribution, which we in most cases do not. For n data points, we can instead use the *empirical error*:

$$\mathbb{E}_E[h] = \frac{1}{n}\sum_i^n \mathcal{C}(h(x_i), y_i). \tag{7.4}$$

With the expected and empirical errors, we can compute the *generalization error* as the difference between those two:

$$G = \mathbb{E}[h] - \mathbb{E}_E[h]. \tag{7.5}$$

In the limit of the generalization error goes towards zero,

$$\lim_{n\to\infty} G = 0,$$

we say that an algorithm can learn or generalize from the data. In general, we cannot compute the generalization error since we in general cannot compute the expectation error. To solve this we can divide our data set into training and test sets, and then use cross-validation to estimate the generalization error. The values on the cost function on the training and test sets are called the *in-sample* error, E_{in}, and *out-of-sample* error, E_{out}, respectively. The in-sample error can be an appropriate approximation to the generalization error if the data set is large enough and is representative of the function f.

In Figure 7.1 we see how the errors in general behave when the training set size or number of data points increases. We have assumed here that the number of data points is not small and that the true function $f(x)$ can't be exactly fit. As the number of data points increase, we see that the in-sample error increases while the out-of-sample error decreases. The sampling noise decreases since the error difference between the two errors decreases. The out-of-sample error we get from this sampling noise is called the *variance*, which goes towards zero in the infinite data limit. As the training data set approaches the infinity limit, we can conclude that the two errors must go to the same value. This is called the model *bias*. The bias is a representation of the best our model can do with infinite data size.

7.2.2 Bias-Variance Decomposition

We will now go a bit further into the bias and variance that is an important aspect of machine learning. Lets consider a data set $\mathcal{D}(\mathbf{X}, \mathbf{y})$ with N pairs

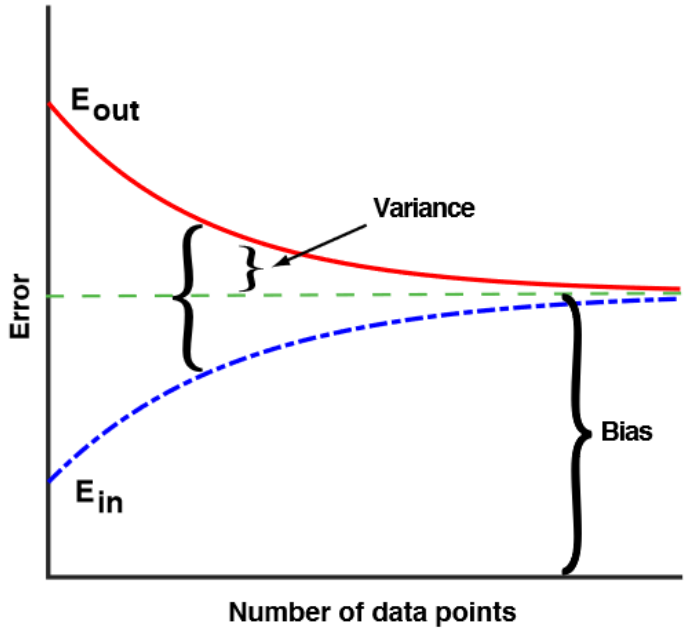

Figure 7.1: Illustration of the in-sample error, E_{in}, out-of-sample error, E_{out}, variance, bias and difference of errors as function of the training set size. It is assumed that the number of data points is not small, and that we cannot exactly fit the true function $f(x)$. The training error increases while the test error decreases as the training set size increases. Figure is taken from ref. Mehta et al. [58].

of independent and dependent variables. We then assume that the true data is created from a noise model

$$y = f(x) + \epsilon, \tag{7.6}$$

where ϵ is a normally distributed noise with mean zero and standard deviation σ_ϵ. A chosen estimator $f(\mathbf{x}; \hat{\theta})$ is trained by minimizing the cost function, lets say the sum of squared errors[2],

$$\mathcal{C}(\mathbf{y}, f(\mathbf{X}; \theta)) = \sum_i (y_i - f(\mathbf{x}_i; \theta))^2. \tag{7.7}$$

Our best estimates for the model parameters,

$$\hat{\theta}_{\mathcal{D}} = \underset{\theta}{\text{argmin}} \, \{\mathcal{C}(\mathbf{y}, f(\mathbf{X}; \theta))\}, \tag{7.8}$$

[2]This is used in regression cases. For classification we could use cross-entropy for instance.

are functions of the data set $\mathcal{D}$. Then we make another set of data sets $\mathcal{D}_n = (\mathbf{y}_n, \mathbf{X}; n)$, where all sets have N samples. We want the expectation value, $\mathbb{E}_{\mathcal{D}}$, of the cost function of all these data sets. We also want the expectation value of the average over different noise instances $\mathbb{E}_\epsilon$. The expected generalization error can be found to be (full derivation can be seen in Appendix A):

$$\begin{aligned}\mathbb{E}_{\mathcal{D},\epsilon}[\mathcal{C}(\mathbf{y}, f(\mathbf{X}; \hat{\theta}_{\mathcal{D}}))] = &\sum_i (f(\mathbf{x}_i) - \mathbb{E}_{\mathcal{D}}[f(\mathbf{x}_i; \hat{\theta}_{\mathcal{D}})])^2 \\ &+ \sum_i \mathbb{E}_{\mathcal{D}}[\{f(\mathbf{x}_i; \hat{\theta}_{\mathcal{D}}) - \mathbb{E}[f(\mathbf{x}_i; \hat{\theta}_{\mathcal{D}})]\}^2] \\ &+ \sum_i \sigma_\epsilon^2 \end{aligned} \tag{7.9}$$

The first term in equation 7.9 is the bias

$$\text{Bias}^2 = \sum_i (f(\mathbf{x}_i) - \mathbb{E}_{\mathcal{D}}[f(\mathbf{x}_i; \hat{\theta}_{\mathcal{D}})])^2, \tag{7.10}$$

and is a measure of the deviation of the expectation value of the model estimator from the true value. This is the best we can do in the infinity limit as we have already discussed. The second term is the variance

$$\text{Var} = \sum_i \mathbb{E}_{\mathcal{D}}[\{f(\mathbf{x}_i; \hat{\theta}_{\mathcal{D}}) - \mathbb{E}[f(\mathbf{x}_i; \hat{\theta}_{\mathcal{D}})]\}^2], \tag{7.11}$$

and is measures the fluctuation in the estimator due to finite-sample effects. The last term is just a noise term $\text{Noise} = \sum_i \sigma_\epsilon^2$. By combining these three terms we can decompose the out-of-sample error as

$$E_{\text{out}} = \text{Bias}^2 + \text{Var} + \text{Noise}. \tag{7.12}$$

It is often much simpler to train a very complex model than it is to obtain sufficient good data. Therefore it is normally more useful to use a less complex model with higher bias, since it is less sensitive to noise in the sampling data from having a finite-sized training data set.

7.2.3 Bias-Variance Tradeoff

Before we look into classification, we need to be aware of a few problems with supervised learning. First is the balance of variance and bias. This is called the **bias-variance tradeoff** in statistics and machine learning. We want to minimize both the variance and bias such that our model both

works well on unseen data and captures the relations between the features and classes, but when one of them is lowered the other has a tendency to increase. High bias may lead to underfitting between the features and the classes, while high variance may lead to overfitting. When a model is overfit, it is excessively complex and will then model noise in the data as well. Overfit models will then do a great job during fitting, but worse on data outside of the training domain. Underfit models do not have the power to capture important variations in the data. With today's improved machinery, it is often easier to make a model too complex rather than to not.

Second is the amount of training data that is available depending on the real function. For a more simple real function, the model does not need that much training data to learn on. While for a more complex[3] real function, the model needs a lot of training data.

Third is the dimensionality of the features. If there are a lot of features with high dimensionality, the model may be confused and cannot separate out the most important features that defines the output. One way to fix this is to manually remove irrelevant features in the data that can confuse the model. The method for doing this is called **dimensionality reduction**, and there are several strategies for doing this.

The fourth and final major concern is noise or incorrect values in the desired output values. This often comes from human error or errors in sensors which can lead to overfitting. This can be fixed by e.g., remove noise training data or use early stopping. There also exists other factors that one need to consider, but these four bias-variance related issues are some of the biggest.

In Figure 7.2 we see illustrations of the bias-variance tradeoff for training error, E_{in}, and test error, E_{out}, as the model complexity increases. In Figure 7.2a we see that as the model complexity increases, the model fits the training data well leading to high variance. For a low complexity model the bias is high. This is exactly as we have already look at above. So we want a model that has a compromise between the variance and the bias, as seen by the optimal line in Figure 7.2a. This optimal line is also where we have a minimum in E_{out}. For the prediction error for test and training samples in Figure 7.2b as function of the model complexity, we see the variance and bias areas for low and high model complexities. From the gap between the two prediction error samples we see the same argument for choosing a optimal compromise between variance and bias. This will lead to a predicted error difference between training and test samples that is not to big and not to

[3]When we talk about simple and complex real function, we mean the complexity of interactions between the features and the number of features we use to approximate the true function.

similar to each other. Often we want to use a more biased model with small variance to minimize E_{out} and maximize the predictions.

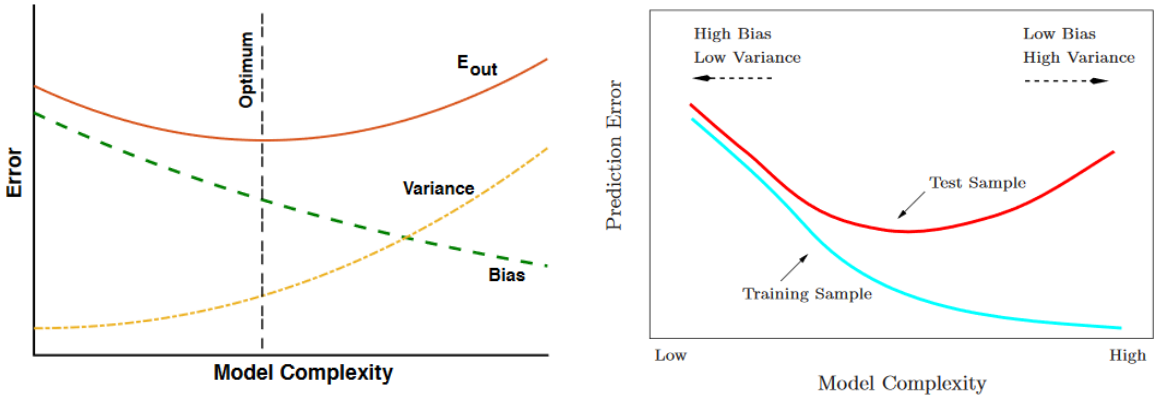

(a) (b)

Figure 7.2: Illustrations of the bias-variance tradeoff as function of model complexity. From these two illustrations we see that we want to find the optimal compromise between variance and bias that gives the best model, which does not underfit nor overfit the data. Figures are taken from ref. Hastie et al. [57] and Mehta et al. [58].

7.2.4 Regularization

With increasing data power and an increase in the amount of data collected today, the data sets we can gather can be quite complex. This also gives need for better machine learning models. With these better models we can solve more complex problems than before. As we mentioned earlier, this also gives rise to more problems, especially overfitting models. Ovefitting is a more common issue than underfitting, since overfitting comes from that the models fit functions and training data too well, making it perform worse on unseen (test) data. This is not something we desire to get, since machine learning is all about training model to analyze new data.

Finding good methods to reduce overfitting has been an important aspect in machine learning a long time. That is the reason for developing *regularization* techniques that reduces overfitting problems without significantly worsen the performance on the training data. Regularization techniques try to improve the generalization error of the test set. There are several different regularization methods that can be used, depending on the type of models that are used.

One way is to tune the model complexity to be better at predicting. This is done by introducing a penalty for individual weights, w . There are two types of norms of regularization that is often used; L1 and L2:

$$L_{1,\text{norm}} = \sum_i |w_i| \tag{7.13}$$

$$L_{2,\text{norm}} = \sum_i ||w_i||^2 \tag{7.14}$$

The L1 penalty will yield sparse feature vectors from the fact that most features weights will be zero. That means that the L1 norm can be seen as a kind of feature selection that removes irrelevant features in data sets with higher dimensionality that would only confuse the model when training. This feature reduction can also be done manually by removing the irrelevant features that makes the model underperform, making it less complex. The L2 norm also acts on the weights of the loss function. These two regularization norms are set in the models as *hyperparameters*.

Other ways to avoid overfitting is to *prune* the models that uses *trees*[4], which affects the splits in the making of trees. *Sampling* and *early stopping* are also other ways to control overfitting by making boosted trees less correlated and stop training when a chosen training metric of a model no longer improves, respectively. All these ways to control overfitting are controlled by various input parameters numerically.

7.2.5 Hyperparameters

As we have already mentioned, hyperparameters are something that have to be manually chosen before fitting a model. The reason for hyperparameters is to tune and optimize the models to do a better fit on the data. They are used to control the algorithms. These hyperparameters have no strict solution and change depending on the data set we are looking at. The same type of parameter may not have the same value in different models as well. For a small set of hyperparameters we could simply use trail and error to test the parameters. Most modern models require a lot of different hyperparameters. When there are a lot of parameters to tune, we may want to use some learning algorithm that searches through some given sets of hyperparameter values. An efficient method for doing this is to do a random search that uses the fact that not all hyperparameters will be as important. Searching for parameters are often computationally expensive since they require that the model is re-trained each time we change a configuration of hyperparameters.

[4]We will come back to what this is later.

During the hyperparameters optimization, we want the test set to be isolated until the model is fully optimized. This is where the validation set becomes useful. The purpose of the validation set is to be used when training the model and optimize the hyperparameters. The first split of the original data set is into training and test sets. Then the training set can then be further split into a smaller training set and a validation set. This means that we loose some training data which we need to take into consideration. The evaluation of the validation set will not be the exact same as evaluating the test set. The generalization error of the test set will be underestimated by the validation set error since the hyperparameters are trained on the validation set.

7.3 Classification

Classification is one of the most used and most successful tasks in machine learning. Classification uses algorithms to decide which category the input belongs to. The function that produces an output value can instead be used to produce a probability distribution over the different outcomes. The simplest and probably most common classification problems are binary outcomes like True or False, Yes or No, Cat or Dog etc, where the outcomes are either the one or the other. When there are more than two outcomes, or classes as they are called, we use multiclass classification algorithms. Not all classification algorithms are made to classify instances with more than two outcomes, and cannot be used to classify problems other than binary outcomes by itself. On the other hand, they can be turned into multiclassifiers by using various strategies. There are also other types of classifiers that are similar to multiclass classifiers, like multilabel and multioutput classification. They are similar, but are used in different cases with different outcomes. For example, multiclass classification only labels a sample as one class only, meaning that it cannot be classified with two classes. This means that an image of a cat can only be classified as either a "cat" or a "dog" by the algorithm. The other two may categorize the image as both a "cat" and as "small" for instance.

In this thesis, we use multiclass classification to classify different particles in event decay chains produced by colliding two protons together many times like at the LHC. To do the multiclass classification in this thesis we will test different classification models and algorithms with various values for the hyperparameters for the respective models, to try and optimize and find the most accurate model. We will also study various evaluation metrics used to both find and evaluate the performance with the best model.

7.4 Classification Models

A so-called "hard" classifier will assign each datapoint to a category, while a "soft" classifier will give the probability of a given category. The simplest classification algorithm is the "perceptron". It is given by the same transformation as linear regression with a weight matrix $\mathbf{w}$,

$$\mathbf{y} = \mathbf{X}\mathbf{w}. \tag{7.15}$$

The classes are then determined by the sign of the predictions by using sign functions or use boundary thresholds. The perceptron is an example of a "hard" classifier. Sometimes it may be useful to use a "soft" classifier yielding category probabilities instead.

There are a lot of different classification models in machine learning with their own strengths and weaknesses. This is why we in this thesis will test a few different approaches and algorithms to find the best model for the analysis. In this section, we will briefly look at the classification methods we will test in this thesis.

7.4.1 Logistic Regression

A simple "soft" model in statistical analysis for classifying discrete outcomes is logistic regression (LR)[58]. It uses linear regression to fit data and a logistic function[5], usually the Sigmoid function

$$\sigma(s) = \frac{1}{1 + e^{-s}}, \tag{7.16}$$

to predict the outcomes into categories by using probabilities. A threshold for the predicted values is chosen which determines which classes the data belongs to. These boundary thresholds can be complex and doesn't have to be linear. The cost function is the usually the cross-entropy with added L_1 (eq.7.13) and L_2 (eq.7.14) regularization terms. The cross-entropy is the negative log-likelihood of the prediction being in the data set. The cross-entropy is derived from the fact that the Maximum Likelihood Estimator (MLE) is the set of parameters that maximize the log-likelihood.

The most basic model is a Binary Logistic Regression that yields two possible outcomes. However, it can be extended to more than two outcomes by using Multinomial Logistic Regression. LR can also be combined with cross-validation using various optimization solvers supporting the regularization parameters.

[5] It can also be called an activation function.

7.4.2 Ridge Classifier

The Ridge classifier uses ordinary Ridge regression[59] after converting the outcome values into a range of {-1,1}, treating it like a regression case. The Ridge classifier uses a Least Squares loss for fitting the model by introducing a penalty to the Ordinary Least Squares (OLS) normally used in Linear Regression. The penalty uses a complexity coefficient, α, that acts as a shrinkage (regularization) parameter that acts on the linearity of the coefficients.

In the case of a multiclass case, the classifier uses multi-output regression as an extension. It will use a one-versus-all approach, where n, corresponding to how many classes we have, classifiers are trained. Computational advantages in the Ridge classifier can lead to a speed advantage over LR for many classes. It can also be combined with cross-validation like LR.

7.4.3 Support Vector Machine

Support Vector Machines (SVMs)[60] try to construct an optimal hyperplane for the K features in the data, making a K-dimensional space, separating the data points in the target classes. When the maximum distance separating the class data have been reached, we have the optimal hyperplane. The hyperplane is affected by *support vectors*, which are the data points that are closest to the hyperplane. The SVM is similar to LR in that it takes the output from a linear function, but assigns the values in the range {-1,1} like the Ridge classifier. Then a cost function with a regularization parameter is used to maximize the margin between the hyperplane and the data points. The regularization parameter is used to balance the loss and the maximization of th margin. A "soft" margin is introduced to account for misclassification by adding a loss to the regularization parameters. A kernel function is then used to increase the dimensional space and (hopefully) improving the hyperplane.

SVM also supports multiclass classification by changing to several binary classification problems. One method is by implementing a one-versus-one (7.4.13) scheme creating one classifier and trains on two classes at a time, creating many classifiers in total. It can be altered to instead use a one-vs-rest (7.4.13) scheme with a separate classifier for each class.

7.4.4 Multi-Layer Perceptron

A Multi-Layer Perceptron (MLP)[61] is an artificial feed-forward neural network (FFNN) model, and is similar to LR in that it has an *input* and an

output layer, but differs in that between these layers (also called nodes), the MLP can have several non-linear layers called *hidden layers*. As a FFNN, the information only goes one way. The inputs are called neurons and are transformed in the hidden layers by a weighted linear summation of the inputs and a non-linear activation function to determine the outputs for each layer. The hidden layers often have some bias to ensure non-zero values. The output layer transforms the values from the last hidden layer into output values. In Figure 7.3a we see how each node in a neural network is connected to all the nodes in the previous layer with a weight value. Then it goes to a non-linear activation function that transforms the node to an output either to a new node in a hidden layer or to the output layer. The nodes will also have some bias terms connected as well. In Figure 7.3b we see a fully connected neural network since all nodes are connected to all nodes in the next layer.

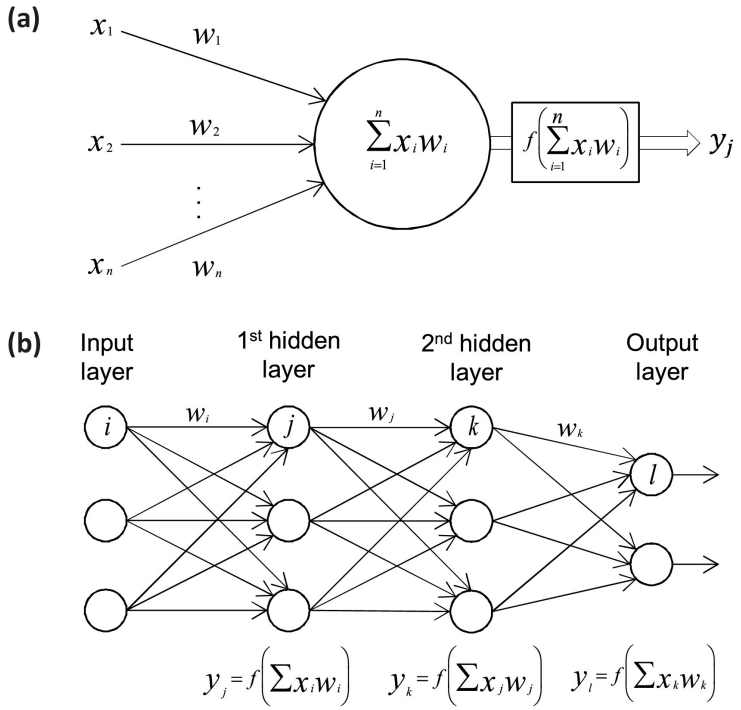

Figure 7.3: (a) Each node in a neural network has some input acted on by some associated weights. Then the weighted inputs are summed together inside the node a passed to a non-linear activation function that transforms it to an output. (b) This is a FFNN/MLP with 3 inputs, 2 hidden layers and 2 classes. All the nodes in one layer in connected to all the node in the next layer. This is then a fully connected neural network. Figure is taken from ref. Vieira et al. [62].

The MLP trains the model using *backpropagation* and with initial guesses for the biases and weights. Backpropagation is a method that is used to optimize the weights and biases to minimize he cost function. The backpropagation iterates backwards from the last layer to the first layers to do this process and is based on gradient descent of the weights and biases. The new biases and weights are then used to start a new feed-forward process from the input layer. This process is repeated until the cost function is sufficiently minimized.

There are a few typical choices of activation functions, which include the hyperbolic tangent function, the sigmoid and the rectified linear unit function (ReLU). The choice of cost function is also something that has to be considered. The MLP library by *Scikit-Learn*, only supports the cross-entropy loss function as the cost function. The logistic loss function is also a good choice of loss function as well.

Neural networks have a large amount of parameters that often leads the network to overfit the data. That is why we also here add a L_2 regularization penalty to the weights, like with Ridge. This hyperparameter have to be tuned. Another hyperparameter that is needed is the *learning rate*. This parameter is used to control the step length in the optimization of the cost function with a gradient descent method. In this case, the weights and biases are the parameters to be adjusted while this is something else in other models. There are a few gradient descent methods we could use like stochastic gradient descent with minibathces to avoid the possibility of interpreting a local minimum as a global minimum. A more modern method is the *adam* solver proposed by Kingma and Ba [63]. It is a stochastic gradient-based optimizer which combines batched data, momentum and adaptive learning rates and adds a few more hyperparameters to be tuned, β_1, β_2 and ϵ.

For multiclass classification, the softmax function is used as the last hidden layer activation function. It normalizes the output of the network into a probability distribution over the predicted output classes.

7.4.5 Decision Tree

Decision Trees (DTs)[64] tries to learn simple decision rules from the data features to construct a tree-like model to predict the target values. The model simply tries to break down a complex decision into several simpler decisions. Each tree starts of with a single *root* node containing all the class labels. The root node then splits into several smaller *internal* nodes, which then splits into *leaf* nodes in the end representing the class targets. The splits are decided by some chosen *criterion* function that uses some strategy to do the splits. The root node is chosen as the feature with the highest

information gain value by the criterion function. The path from the root node to an internal node or a leaf is always unique, and the leaves do not have any descendants.

The DT uses a cost function to determine the the most homogeneous branch when splitting. The stopping point for splitting is something we can decide as an input parameter to the model by choosing a maximum depth of the tree from the root to the leaves, or set the maximum number of leaves to have at the end. Other parameters for controlling the size and splitting of the tree are to be considered as well since the DT is prone to overfitting with many features. This can be fixed by pruning the tree to remove nodes with low importance features, use dimensionality reduction with e.g. principal component analysis (PCA)[65] or decrease some of the controlling parameters.

There are a few different DT algorithms to generate the optimal trees. The algorithm that is implemented by scikit-learn is an optimized version of the Classification and Regression Trees (CART) algorithm that construct binary trees from the features and thresholds for giving the highest information gain at each node. The scikit-learn DT classifier automatically supports multiclass classification as well.

7.4.6 Bagging

Bagging[66] is an ensemble method that uses several base estimators independently, with a chosen classifier, and takes the average of their predictions. E.g. the base estimator could be a DT such that the bagging classifier would make several decision trees and combine them to improve the accuracy score and reduce the variance of the estimator. This is normally better than using only one of the base estimator alone. The base classifiers are fit on random subsets of the training data together with bootstrap aggregation.

There are more bagging methods that depend on the strategy of how they draw the random subsets of the training set. The Bagging strategy is when the samples are dawn with replacement. Other strategies are Pasting, Random Subsets and Random Patches. With bagging we can control the size of the subsets and if we want to draw with replacement or not of samples and features.

7.4.7 Random Forest

Another classification ensemble method is the Random Forest (RnF)[67] algorithm. It produces a number of DT classifiers on bootstrapped training samples with a low correlation to each other, and uses their average like

the bagging method. This improves the accuracy score and helps control overfitting. Can also choose to bootstrap samples or not.

Like with the DT algorithm, we can control the size and splitting of the tree. These two algorithms are very similar and have many of the same input parameters and same procedure for building the trees. The main difference is that with the RnF algorithm, we produce many trees with sources of randomness. This randomness is very important in that it decreases the variance when combining and taking the average of many trees, and can cancel out some prediction errors. This normally yields a better model.

7.4.8 AdaBoost

Instead of using average ensembles where we use many independent bootstrap samples, we can use something called *boosting*. This is a type of method that keeps the weight for each instance and the base estimators are built sequentially. It then builds a combined estimator that reduces the bias. The result is to get a powerful ensemble from several weaker models combined.

One such boosting method is the AdaBoost classifier[66][68]. The AdaBoost uses adaptive boosting and weaker classifiers as estimators to sequentially combine them into a single better classifier with a weighted majority. It will fit weaker classifiers sequentially such that the next classifier will have a different weight than the previous to adjust for incorrect classification in the previous. Data that are difficult to predict will then have an increasing influence since the next classifier will learn from the mistakes of the previous weaker classifier. The final prediction is the result of a weighted majority vote of the combination of the weaker classifier predictions. A weaker classifier can then be boosted to a stronger classifier that is more accurate at predicting.

The AdaBoost algorithm by scikit-learn takes a weaker classification algorithm as input together with the maximum number of estimators to be boosted before stopping. If the model is to be perfectly fit, the executing will also be stopped. It also takes a learning rate parameter for the shrinking of the classifiers. The AdaBoost algorithm can naturally detect and adapt to a multiclass problem.

7.4.9 Gradient Boosting

Gradient Boosting Decision Tree (GBDT)[69] is another boosting method like AdaBoost. The GBDT is an additive model that tries to identify the shortcomings of the weak classifiers. While AdaBoost uses high weight data points, the GBDT uses the same for gradients in the loss function. This

lets the cost function to be more specified for optimization for fitting the classification problem. The K number of regression trees[6] at each stage are fit on the negative gradient of the binomial (binary class) or multinomial (multiclass) deviance loss function.

The algorithm is well suited for both binary and multiclass classification, and takes the maximum number of estimators and the learning rate as input parameters. Since it is a boosted tree method, it can also take the maximum depth of the trees and maximum number of leaves as inputs. It is also quite robust to overfitting. When we have a multiclass problem, the algorithm will create K trees for each iteration when we have K classes. The loss function for multiclass also have to be "deviance" to give probabilistic outputs (similar to LR).

When dealing with larger data sets (n_samples>10 000) or have a larger number of classes, a histogram-based gradient estimator can be more useful. Scikit-learn has an experimental implementation of GBDTs called **HistGradientBoostingClassifier** which is inspired by Ke et al. [70] on a **LightGBM** algorithm. This estimator can be orders of magnitude faster than the original GBDT estimator. To reduce the computation time and number of splitting points, the algorithm bins the input samples into integer-valued bins. They share most of the same parameter inputs that controls the models, except that the histogram-based estimator gets a parameter for controlling the number of bins. This can act as another regularization parameter.

7.4.10 Extreme Gradient Boosting

Another highly efficient, flexible and portable tree boosting method is the Extreme Gradient Boosting (XGBoost)[71]. It is a scalable end-to-end tree boosting system that is an optimized distributed gradient boosting algorithm. It provides fast and accurate parallel tree boosting. It is one of the most used and highly recognized machine learning algorithms today together with deep neural networks. One of the most important aspects of the XGBoost is its scalability, making it several times faster than other algorithms combined with parallelization.

The XGBoost algorithm uses the GBDT framework as its core and the potential loss for the possible splits to make a new branch as it looks at distributions of the features for all data points in a leaf to build trees. This decreases the space of possible feature splits search. The algorithm chooses which features and split-points that maximizes the gain. The splits are binary such that it splits according to if a value is bigger or lower than a set threshold

[6]For a binary classification case, only a single tree is fit.

cut by the algorithm. The gain is different depending on the type of loss function that is used. With a small data set (number of rows $\leq$ 4'194'303, set by default), the XGBoost algorithm tries all split points gained by the data values for each feature. The feature and threshold combination with the highest gain is then chosen. For a larger data set, the algorithm uses fewer candidate splits given by the quantiles of the data.

Since this algorithm is more complex than other techniques, it also requires more parameters to be tuned to control the model properly. The parameters can be sorted into *general parameters* for choosing the booster method, *booster parameters* that are dependent on the boosting method and *task parameters* that specify learning task parameters and learning objective. We are using a tree booster that has many of the same tree boosting parameters like the DT and RnF algorithms like regularization terms, hyperparameters for tree controlling, pruning and others. The task parameters consist of the type and size of classes we have, like multiclass classification, and types of evaluation metrics to use.

7.4.11 Light Gradient Boosting Machine

Light Gradient Boosting Machine (LGBM)[70] is a distributed gradient boosting framework for machine learning. It is similar to the XGBoost algorithm, but it is made to be faster, around 7 times faster, with higher efficiency, lower memory usage and better accuracy. This is a huge advantage when dealing with larger data sets. The LGBM algorithm uses a gradient based one-side sampling for filtering the data samples to find the split value in the trees, while the XGBoost uses a histogram based algorithm to find the best splits. They have very similar input parameters for the algorithms.

7.4.12 Voting Classifier

Most machine learning algorithms have their own weaknesses when modeling and fitting data sets. A method for balancing out these weaknesses is the combination of several different types of (previously unfitted) classifiers that use some voting technique to exploit different traits from the classifiers to even out the weaknesses. The goal is to increase the accuracy score of the models as one better model. This idea is called a Voting classifier[72][73], and uses two types of voting techniques to predict the classes; a majority (hard) vote and an average predicted probability (soft) vote.

The hard voting uses the predicted class labels for majority rule voting. The classified sample by the model is then the majority class label of the classifiers combined. The soft voting uses the *argmax* of the sums of the

predicted probabilities to predict the class labels. This is most preferred when using an ensemble of equally well performing classifiers. Both have the option to add a sequence of weights to weight the different classifiers. The predicted classes and class probabilities are then multiplied with the corresponding weight and averaged. The class with the highest average is then chosen as the class label. The Voting classifier also supports individual classifier hyperparameter tuning with some hyperparameter search algorithm. It also supports multiclass classification as long as the provided classifiers support multiclass classification.

7.4.13 Multiclass Classification Models

To do multiclass classification, there are several existing techniques. We will look more into two of those techniques[7]; transformation to binary and extension from binary. These are all meta-estimators. This means that they all need a base estimator, most often a binary classifier, which is extended to do multiclass classification when they are implemented in the constructors.

The extension from binary technique is rather trivial. We simply use already existing binary classifiers and modify them to do multiclass classification. Not all binary classifiers can be extended beyond binary though. The classification models we looked at in the last section **??** can either do this automatically, or have input parameters and constraints in the models that have to tell the models to do multiclass classification in some way.

Transformation to binary reduces our multiclass problem down to several binary classification problems. This technique can also be split into more strategies, which we will look more into.

One-Vs-Rest Classifier

The first strategy is the one-vs-rest (OvR) classifier. Each class in this model has its own classifier that does the fitting, and the classifier fits the single class against the rest of the classes. This means we only need n classifiers for the n classes. This also improves interpretability, since we can get information about a specific class by looking at its classifier.

The OvR takes a binary classifier along with samples and targets as inputs and outputs a list of the classifiers for each class. When doing the predictions, it uses all the classifiers on unseen data where it picks the class with the highest confidence score as prediction.

[7]There is also a third technique, hierarchical classification, that we do not look at.

One-Vs-One Classifier

The second strategy is the one-vs-one (OvO) classifier. This takes one classifier and a pair of classes at a time. For each pair of classes, the classifier trains on data containing these classes and must learn to distinguish them. This happens between all the classes. It then uses a voting scheme to select the class with the most votes when predicting. For n number of classes in the multiclass problem, the OvO trains $n(n-1)/2$ binary classifiers. All the classifiers that are trained here will be applied when doing the prediction on unseen data, and the one with the highest number of predictions will be predicted by the combination of classifiers.

This method is of course slower than the OvR since it has a $\mathcal{O}(n^2)$ complexity. Both these two methods do suffer from that there may be regions where the input space can get the same number of votes.

7.5 *Evaluation Metrics

To evaluate the performance of the classification models properly and decide which model fits the data the best, we need to have some evaluation metrics that we can use. In this section we will take a look at the evaluation metrics we will use for the classification[8].

7.5.1 Mutual Information

To look closer at the correlations in the data set, we can use the entropy and information gain. The entropy can be calculated by using the probability $P(j)$ of a value j occurring when j is a value that a feature group x_i can take;

$$H(x_i) = -\sum_{j \in x_i} P(j) \log_2 P(j) \tag{7.17}$$

With a given target $\mathbf{y}$, we can calculate the conditional entropy of a feature x_i:

$$H(x_i|\mathbf{y}) = -\sum_{y \in \mathbf{y}} P(y) \sum_{j \in x_i} P(j|y) \log_2 P(j|y) \tag{7.18}$$

Now we can compute the information gain, or *mutual information* in the context of variable selection, for a given feature as the difference between these two entropies:

$$I(x_i : \mathbf{y}) = H(x_i) - H(x_i|\mathbf{y}) \tag{7.19}$$

[8]See Scikit-Learn[75] for more details on metrics.

With the information gain we get a measure of the correlation between a feature and the target, which detects non-linearities or the amount of information that one feature provides about another.

7.5.2 Accuracy Score

To measure the performance of the models, we use the the accuracy score for classification. This is a measure of how well the models can predict the classes. It is defined as the number of correct predictions divided by the total number of predictions, giving a value between 0 and 1.

$$\text{Accuracy} = \frac{\sum_{i=1}^{n} I(\tilde{y}_i = y_i)}{n} \tag{7.20}$$

$\tilde{y}_i$ is the predicted target by the model, y_i is the actual class target, n is the total number of predictions and I is and indicator function

$$I = \begin{cases} 1, & \text{if } \tilde{y}_i = y_i \\ 0, & \text{if } \tilde{y}_i \neq y_i \end{cases} \tag{7.21}$$

When the model prediction fits the data perfectly, we get an optimal score of 1.

The accuracy score can be computed for all data sets, training validation and test sets. If there is a big difference between the accuracy score for either validation or test and training, we might under- or overfit the data. When the training score is much better, we most likely overfit the data, and might have to something to change that by regularization or tuning hyperparameters.

Another way to balance out the accuracy scores is to use *cross-validation*. Is is a very useful technique against overfitting or to tune hyperparameters. There are several cross-validation techniques, but the main idea of cross-validation is to divide samples into subsets. It will then do the analysis on one subset and compute the accuracy. Then it will do another analysis with another subset to get a different accuracy. After many rounds of dividing the data into subsets and computing several accuracy scores, the average score is used as an estimate of the model performance. The Scikit-Learn library has a function called *cross_val_score* that does this, and we can choose how many folds of subsets we want the data to be split into.

7.5.3 Cohen Kappa Score

Another scoring statistic is the Cohen Kappa Score (CKS)[74]. The CKS measures the interrater reliability, which takes into account what the accuracy could have been through random predictions. This comes from that

perfect agreement is not something that usually happens. It accounts for uncertainties in the predictions as from a random classifier vs a more accurate and tuned classifier on the classes. An example is that different human data collectors can interpret data differently from more vague variables, which then affects the data collection and outcomes. As for the accuracy score, 1 is the optimal score, but it ranges from -1 to 1 like many other correlation statistics. It is calculated as

$$\kappa = \frac{\text{Observed Accuracy} - \text{Expected Accuracy}}{1 - \text{Expected Accuracy}} = \frac{p_a - p_e}{1 - p_e} \tag{7.22}$$

7.5.4 Error Evaluation

To evaluate the error as best as we can, we will use a few different error metrics to get a good overall error estimate of the classification models. These will also help to discover any over- or underfitting of the data.

Error Rate

With the accuracy score, we can compute the *error rate*. The error rate is defined as the fraction of misclassification cases the model has on a data set:

$$\text{error} = 1 - \text{accuracy} \tag{7.23}$$

This is an often used metric in classification. Both the error and the accuracy score can be computed in multiclass classification cases.

Log Loss

Instead of using discrete predictions, we can evaluate probability outputs of classifiers. We can use the *log loss* function, also called the cross-entropy or logistic regression loss, to do this. When dealing with a binary case with a probability estimate $p = P(y = 1)$, the log loss is defined as the negative log-likelihood given a true output for each sample. It is computed as

$$L_{\log} = -\log P(y|p) = -(y \log(p) + (1 - y) \log(1 - p)). \tag{7.24}$$

For a multiclass case, the log loss is taken over a whole set of K labels with a 1-of-K binary indicator matrix $\mathbf{Y}$ and a matrix $\mathbf{Pr}$ of probability estimates as

$$L_{\log}(\mathbf{Y}, \mathbf{Pr}) = -\log P(\mathbf{Y}, \mathbf{Pr}) = -\frac{1}{n} \sum_{i=1}^{n} \sum_{k=1}^{K} y_{i,k} \log p_{i,k}. \tag{7.25}$$

Variance

Previously in section 7.2.2 we defined the variance and the bias of a model. These two are used to check for under- and overfitting of the data set by our model(s). The variance is a measure of how far the spread of our predictions are from their average values. Given the predictions, $\tilde{\mathbf{y}}$, of a model, the variance is calculated as

$$\text{Var}(\tilde{\mathbf{y}}) = \frac{1}{n}\sum_{i=1}^{n}(\tilde{y}_i - \frac{1}{n}\sum_{j=1}^{n}\tilde{y}_j)^2. \tag{7.26}$$

Bias

The bias error is a measure of the difference between the true values, $\mathbf{y}$, and the average of the predicted values. To get the out-of-sample error in equation 7.12, we used the bias squared. This can be calculated as

$$\text{Bias}^2(\mathbf{y}, \tilde{\mathbf{y}}) = \frac{1}{n}\sum_{i=1}^{n}(y_i - \frac{1}{n}\sum_{j=1}^{n}\tilde{y}_j)^2. \tag{7.27}$$

7.5.5 Classification Report

With Scikit-Learn, we can easily build what is called a *classification report*. This is a text report containing some useful classification metrics by using the true targets and predictions by the model.

First we will look at some useful prediction results used to compute some of the report metrics:

Positive (P) - The observation is positive.

Negative (N) - The observation is negative.

True Positive (TP) - Observation is positive, and the prediction is positive.

True Negative (TN) - Observation is negative, and the prediction is negative.

False Positive (FP) - Observation is negative, but the prediction is positive.

False Negative (FN) - Observation is positive, but the prediction is negative.

With the last four outcomes above, we can compute some useful metrics in the report:

Precision - The fraction of a sample classified correctly as positive of all positive predicted samples by the model:

$$\frac{TP}{TP + FP}$$

Recall - The fraction of a sample classified correctly as positive of all positive observations (true positive rate):

$$\frac{TP}{TP + FN}$$

The recall of the positive class is also called the sensitivity. The recall of the negative class (true negative rate) is called the specificity.

F1-score - A weighted average of the precision and recall:

$$2 \times \frac{\text{Precision} \times \text{Recall}}{\text{Precision} + \text{Recall}}$$

In the multiclass case, these metrics are computed for each class independently.

The classification report also includes for various classification cases:

Support - The number of true classes in the data set for each class.

Accuracy - The accuracy score of the model (binary case).

Macro avg - Average of the unweighted mean for each class.

Micro avg - Average of the total true positives, false negatives and false positives (multiclass or multilabel cases).

Weighted avg - Average of the support-weighted mean for each class.

Sample avg - Average of samples (multilabel case).

7.5.6 *Confusion Matrix*

...

7.5.7 *Balanced Accuracy*

7.5.8 *Kolomogorov-Smirnoff Statistics*

7.5.9 *Feature Importance*

7.5.10 *ROC Curve*

7.5.11 *Precision-Recall Curve*

...

Part II

*Implementation

Chapter 8

Methods-Overview

In this part, we will look at the framework for the classification we are doing with different models in this thesis. First we will take a look at the data we are using, how they are made before we use them and how the data will look like after we convert them to be used for our work. Since the data we are using are already produced beforehand as Root files, we will convert the data into data frames with Python and make new additional features as well as the targets from the data file(s). The data will then be preprocessed and analyzed before they are split into training, validation and test sets. We will then go through some of the tuning that is done with the models and the validation set and use the evaluation metrics from section 7.5, before we use the best fit model on unseen data.

Python is used for easy implementation of machine learning libraries with Scikit-Learn and plotting using the matplotlib package, as well as other useful libraries we will use. In the following section, we will give a brief presentation of the Python packages that we use in our code.

8.1 Python packages

Before we look at the data and implementation of the models and codes in the next chapters, we will introduce the most important Python packages we are actively using in this thesis. Many of the packages require other packages to be installed, but they do not have to be explicitly imported in the code itself. The codes and necessary requirements, like package versions[1], we use are found at a GitHub repository[2], with more explanations on how to setup

[1]NB!: Some of the used package versions in this thesis will be updated or changed after some time. Check *requirements.txt* for latest current versions when this thesis was written.

[2]GitHub repository: https://github.com/krilangs/ComPhys—Master

and run the codes in a README file. We also import smaller packages with simple functions that we will use, but we will not explain those.

When we present code snippets in this thesis, we will leave out some parts (noted by "\\...") since it will only be used for presentation and visualization of the code used. The full source codes are found at the GitHub repository as mentioned.

- **NumPy**: NumPy, or Numerical Python, is one of the most used packages in Python. It handles arrays, matrices, has functions for working with high-level mathematics, can dump data to files and similar.
- **Pandas**: Pandas is a powerful and easy Python made library for handling data manipulation and analysis. This library is very useful with machine learning for handling the data for visualization since it creates data structures that are flexible, efficient, customizable and easy to use and read.
- **Matplotlib**: Matplotlib is a plotting library for Python and NumPy that creates graphs and visualizations.
- **Seaborn**: Seaborn is a more high-level visualization library, and is based upon matplotlib. It is most used for statistical graphics to understand data better, and is closely connected to pandas.
- **ROOT**: ROOT or PyROOT is ROOT's Python-C++ bindings, lets us use ROOT with Python. This is a very much used in particles physics for using frameworks with the performance of the ROOT C++ libraries. This also lets us use Python libraries like NumPy and Pandas with ROOT.
- **Uproot**: Uproot is a library for converting ROOT files to be used with machine learning libraries with Python and NumPy.
- **Scikit-Learn**: Scikit-Learn[75] is a library most popularly used for data analysis and machine learning in Python. It contains a lot of useful tools for statistical modeling and machine learning.
- **Imblearn**: Imblearn, or Imbalanced-learn, is used with scikit-learn to handle imbalanced data sets in machine learning.
- **XGBoost**: XGBoost is a library that provides a powerful, scalable and distributed gradient boosting framework for machine learning.

- **LightGBM**: LightGBM is another distributed gradient boosting library for machine learning. It is made to be efficient and faster than XGBoost for larger data sets.

Chapter 9

Data

What to have here? Thoughts:

1. An explanation of how the data are produced and simulated, and what machine tools are used to produce these data?
2. Mention/explain/refer to input parameters for producing the data?
3. Explanation of how the data set(s) look?

Chapter 10

*Analyzing the Data

We will now use the data for Monte Carlo produced data, several backgrounds and neutrino signals with a few different scenarios for $N1$ mass, masses of 150 GeV and 450 GeV. We will use an already existing Python script[1] for plotting different property variables of the final state leptons as histograms. We will plot some of the already existing variables in the files, as well as using these to make new angular variables for $d\phi$ and dR. We can then study the variables for the different backgrounds and signal samples. The background and signal samples will later be used to classify the leptons with ML.

The original scripts uses ROOT in Python. We will modify them to suite our case and needs. Since most of the implementations are already there, we only have to modify and add some small things like a few new input parameters and such. This also mostly includes adding the new variables to plot, different data-taking periods and the signal samples that we can plot. The various backgrounds are already implemented and do not need any changes. The modified scripts can be found at the same GitHub repository as before with a README-file for explaining the usage.

The overall layout of the scripts is to make histograms of property variables of the final state leptons in many events for several background samples and neutrino signals, as well as Monte Carlo simulated data, which are stored as ROOT files. We can then look at the differences between the periods the data was taken, the different backgrounds, the difference between the two neutrino signals and between the leptons.

[1] Made by Eli B. Rye.

Chapter 11

Preparing the Data

11.1 Making New Variables

After downloading a data set with the proton-proton collision events, we start by converting it from ROOT to Python syntax with the uproot library and then to a dataframe with Pandas. This is done in the script called *Trilepton_read_root.py*. By using the existing data for momentum and energy for each event and the corresponding four particles in each event, we can use these to compute new useful variables to add to a new dataframe. The new variables we make are the angular variables for each lepton (θ, ϕ, η), angular variables between pairs of leptons ($d\phi$, dR) and the invariant masses of pairs of leptons (m_{ll}), which we talked about in chapter 4. Then we classify the events for making the targets as permutations of the leptons by using their identity traits. The leptons are ordered by decreasing p_T. Since the neutrinos are so small, they will always have the lowest p_T and are then neglected here. The function for making the new variables can be seen in Listing 11.1. The new dataframe is then exported as a .h5-file.

```
# Method for flattening and adding additional variables
def lepaugmentation(df, nlep):
    px  = awkward.fromiter(df['px'])
    py  = awkward.fromiter(df['py'])
    pz  = awkward.fromiter(df['pz'])
    E   = awkward.fromiter(df['E'])
    vtx = awkward.fromiter(df['vtxid'])
    pid = awkward.fromiter(df['pdgid'])

    # Make tlv - handy when computing angular variables
    tlv = uproot_methods.classes.TLorentzVector.TLorentzVectorArray.↩
        from_cartesian(px, py, pz, E)

    df["tlv"] = tlv[:]
```

```
        df["pt"]  = tlv[:].pt
        pt  = awkward.fromiter(df['pt'])
        pt_org  = awkward.fromiter(df['pt'])
        df["phi"] = tlv[:].phi
        phi = awkward.fromiter(df['phi'])

        df["theta"] = tlv.theta
        theta  = awkward.fromiter(df['theta'])

        df["eta"] = tlv.eta
        eta  = awkward.fromiter(df['eta'])

        \\...

        # Make the lepton variables
        for i in range(1,nlep+1):
            df['lep%i_pt'%i]  = pt[pt.argmax()].flatten()
            df['lep%i_phi'%i]  = phi[pt.argmax()].flatten()
            df['lep%i_eta'%i]  = eta[pt.argmax()].flatten()
            df['lep%i_theta'%i]  = theta[pt.argmax()].flatten()
            df['lep%i_px'%i]  = px[pt.argmax()].flatten()
            df['lep%i_py'%i]  = py[pt.argmax()].flatten()
            df['lep%i_pz'%i]  = pz[pt.argmax()].flatten()
            df['lep%i_E'%i]  = E[pt.argmax()].flatten()
            df['lep%i_vtx'%i]   = vtx[pt.argmax()].flatten()
            df['lep%i_pid'%i]   = pid[pt.argmax()].flatten()
            df['lep%i_tlv'%i]   = tlv[pt.argmax()].flatten()

        \\...

        # Compute variables for all combinations of 2 leptons
        pairs = pt_org.argchoose(2)
        print("pairs:", pairs)
        left  = pairs.i0
        right = pairs.i1

        \\...

        for ilep in range(len(left[0])):
            i = left[0][ilep]
            j = right[0][ilep]
            print("i = %i, j = %i"%(i,j))
            idx1 = left[0][i]
            idx2 = right[0][i]
            df['mll_%i%i'%(i+1,j+1)]    = (df["lep%i_tlv"%(i+1)]+df["lep%↩
                i_tlv"%(j+1)]).apply(get_invmass)
            df['dphi_%i%i'%(i+1,j+1)] = df.apply(lambda x : get_deltaPhi(x↩
                ['lep%i_tlv'%(i+1)],x['lep%i_tlv'%(j+1)]), axis=1)
            df['dR_%i%i'%(i+1,j+1)]   = df.apply(lambda x : get_deltaR(x['↩
                lep%i_tlv'%(i+1)],x['lep%i_tlv'%(j+1)]), axis=1)


        df["target"] = df.apply(lambda x : classify_event(x['lep1_vtx'],x[↩
            'lep2_vtx'],x['lep3_vtx'],x['lep4_vtx'],x['lep1_pid'],x['↩
            lep2_pid'],x['lep3_pid'],x['lep4_pid']), axis=1)


        df = df.drop(['px', 'py', 'pz', 'pt', 'E', 'vtxid', 'pdgid', '↩
            evnum','tlv', 'phi', 'theta', 'eta'], axis=1)
        return df
```

Listing 11.1: Making new variables.

11.2 Plotting New Variables

The new dataframe can now be imported by other scripts using Pandas, and used further. With the *Trilepton_plotter.py* script, we import the dataframe for visualization of the variables in it by using the matplotlib library. We make two different function that plots different features. One function plots the *single* variables for each lepton separately in one plot, so one plot can show the p_T for each lepton in one figure by example, while the other function plots the *pair* variables (m_{ll}, $d\phi$, dR). In this way, it is easier to study the variables and properties of the leptons[1]. The figures can then be saved to a desired folder. In Algorithm 1 we see a pseudocode of these two functions.

Algorithm 1 Plotting particle properties.

```
Function:
if input variable is in dataframe then
    Make histogram and figure
    if save is True then
        Save the figure to a folder
    end if
else
    print "Variable not in dataframe"
    print Dataframe
    break
end if
End function
Plot figure(s)
```

11.3 Inspect Data

After importing all the necessary libraries in a new script, *Trilepton_classifier.py*, we load in the dataframes and drop unnecessary features we will not be using. This script will be our main script for doing the classification. Then we make the design matrix $\mathbf{X}$, containing all the particle variables for each event, and the target vector $\mathbf{Y}$, containing all the targets for each event, from the dataframe. The targets are at this point of type *tuples*. This makes classification more difficult, which is why we convert each event target in $\mathbf{Y}$ into an *integer* and make a new target vector $\mathbf{y}$.

[1] This solution was found by testing.

With some useful properties of Pandas dataframes and with Seaborn and Scikit-Learn, we can inspect the variable features a bit more before starting the classification. Pandas dataframes lets us easily print a few lines and a summary of the dataframe. We then get a quick overview of how the data looks like. This includes a short look at the features in the dataframe, like the values for a few events, the names and index dtypes of each feature in the dataframe. It also counts and prints the number of non-null values and the memory usage. Another useful thing to print is the individual target counts to check the number of each target in the dataframe. With this we quickly get an overview to see if we have a balanced or imbalanced data set. This can be very important, since it can lead to problems and we might have to do something to change this before doing the classification.

Correlations

An important descriptive statistic for data analysis with multi-variable data is the *correlation matrix* with Seaborn. It is a symmetric table of size $k \times k$, for k features (this includes the target as well), with pairwise correlations between the features in the data. It summarizes the relationships between the features that we most likely would not have seen by just looking. With machine learning, it is also a good preprocessing step that can give some information to whereas dimensionality reduction might come in handy with high-dimensionality data. The close to 1 the correlation coefficients are, the more correlated are they. We also don't want a value close to -1, since this indicates a strong negative correlation. The diagonal will of course always be 1, since it is the correlation between the feature itself. When a feature has a strong correlation to the target, is has a high significance for predicting the output than a feature close to -1. This helps us exclude features that worsen the prediction. The optimal case is then a high correlation between the independent and dependent variables, while a strong correlation between the independent variables (causing redundancy) is not.

To take a close look at the correlations in the data set, we use the mutual information of the features from section 7.5.1. By using the *mutual_info_classif* function by Scikit-Learn, we can easily compute the information gain of the features and the target. Here, we want the features that maximizes the information gain. This also helps us single out unnecessary features for classification. In the case of decision trees, the information gain is used for the splitting in the trees.

11.4 Preprocessing of the Data

Before we can start with the classification and start choosing the models we will look at, we need to do some preprocessing of the data from the information we got by looking at the data. One aspect we do not have to consider for our data set is NULL values. Since there are no null values in our data, we do not have to do anything about this. We can also check this again quickly by running:

```
df.isnull()   # Returns a boolean matrix, if the value is NaN then↩
    True otherwise False.
df.isnull().sum()   # Returns the column names along with the ↩
    number of NaN values in that particular column.
```

Listing 11.2: Check NULL values.

Resampling

After inspecting the data and the class counts in the target, we make a function using Imblearn for imbalanced data. This allows us to choose between the options of both oversampling and undersampling or only one of them by using boolean input parameters for activating these techniques. This function can be seen in Listing 11.3. This can then balance the data by sampling the information we already have and resample the data set.

```
"""Resample the data to make the datasets more balanced."""
def Resample(X, y, under=False, over=False):
    if under == True:
        print("Undersample")
        undersample = RandomUnderSampler(sampling_strategy="↩
            majority", random_state=42)
        X, y = undersample.fit_resample(X, y)

    if over == True:
        print("Oversample")
        oversample = ADASYN(sampling_strategy="not majority", ↩
            random_state=42)
        X, y = oversample.fit_resample(X, y)

    #print(y.target.value_counts()) # Print the counts of the ↩
        different classes after resampling
    return X, y
```

Listing 11.3: Resample data.

Train, Validation and Test Sets

Regardless of resampling or not, one important thing we have to do with our data when doing classification is to split the data into multiple sets. We split the design matrix $\mathbf{X}$ with the features and the targets $\mathbf{y}$ into three new sets each. This is done by using a Scikit-Learn function called *train_test_split* as seen in Listing 11.4. First we split $\mathbf{X}$ and $\mathbf{y}$ into training and test sets, then we further split the training sets into new smaller training sets and validation sets. 60% of the data are now training, 20% are validation and 20% are test. Remember that the validation set is used to tune the classification models, while the test set is only used as unseen data in the end when we have a good enough fully tuned model.

```
        """Split events into training, validation and test sets."""
        X_train, X_test, y_train, y_test = train_test_split(X, y, ↩
            test_size=0.2, random_state=42, stratify=y)

        X_train, X_val, y_train, y_val = train_test_split(X_train, y_train↩
            , test_size=0.25, random_state=42)
```

Listing 11.4: Splitting the data.

Scaling

The next technique we will apply is scaling of the data. We will use Standardization which means we transform the values with a mean of 0 and a standard deviation of 1. This will fix any unwanted weighting favoring some features. Scikit-Learn has a function for doing this called *StandardScaler*. For the training data we will both fit and transform, meaning that it both calculates the mean and standard deviation and standardizes the data set. We also have to transform the validation and test sets as well, but not fit them. In Listing 11.5 we use the *fit_transform* on the training set, while only using *transform* on the validation and test sets.

```
        """Scale the data when called."""
        def scaler(X_train, X_val, X_test):
            sc = StandardScaler()
            X_train = sc.fit_transform(X_train)
            X_val = sc.transform(X_val)
            X_test = sc.transform(X_test)
            return X_train, X_val, X_test
```

Listing 11.5: Scaling.

Chapter 12

Model Classification

Part III

Results

Chapter 13

**

Part IV

Discussion, Conclusion and Future Prospects

Chapter 14

Discussion

14.1 ?

Chapter 15

Conclusion and Future Work

15.1 Future Work

Part V

Appendices

Appendix A

Bias-Variance Decomposition

Here we do the full derivation of the expected generalization error in equation 7.9:

$$\begin{aligned}
\mathbb{E}_{\mathcal{D},\epsilon}[\mathcal{C}(\mathbf{y}, f(\mathbf{X}; \hat{\theta}_{\mathcal{D}}))] &= \mathbb{E}_{\mathcal{D},\epsilon}\left[\sum_i (y_i - f(\mathbf{x}_i; \hat{\theta}_{\mathcal{D}}))^2\right] \\
&= \mathbb{E}_{\mathcal{D},\epsilon}\left[\sum_i (y_i - f(\mathbf{x}_i; \hat{\theta}_{\mathcal{D}}) - f(\mathbf{x}_i) + f(\mathbf{x}_i))^2\right] \\
&= \sum_i \mathbb{E}_{\epsilon}[(y_i - f(\mathbf{x}_i))^2] + \mathbb{E}_{\mathcal{D},\epsilon}[(f(\mathbf{x}_i) - f(\mathbf{x}_i; \hat{\theta}_{\mathcal{D}}))^2] \\
&\quad + 2\mathbb{E}_{\epsilon}[y_i - f(\mathbf{x}_i)]\mathbb{E}_{\mathcal{D}}[f(\mathbf{x}_i; \hat{\theta}_{\mathcal{D}})] \\
&= \sum_i \sigma_\epsilon^2 + \mathbb{E}_{\mathcal{D}}[(f(\mathbf{x}_i) - f(\mathbf{x}_i; \hat{\theta}_{\mathcal{D}}))^2]
\end{aligned}$$

Here we have used the fact that the noise has zero mean and variance σ_ϵ^2. We also further decompose the second expectation term:

$$\begin{aligned}
\mathbb{E}_{\mathcal{D}}[(f(\mathbf{x}_i) - f(\mathbf{x}_i; \hat{\theta}_{\mathcal{D}}))^2] &= \mathbb{E}_{\mathcal{D}}\left[(f(\mathbf{x}_i) - f(\mathbf{x}_i; \hat{\theta}_{\mathcal{D}}) - \mathbb{E}_{\mathcal{D}}[f(\mathbf{x}_i; \hat{\theta}_{\mathcal{D}})] + \mathbb{E}_{\mathcal{D}}[f(\mathbf{x}_i; \hat{\theta}_{\mathcal{D}})])^2\right] \\
&= (f(\mathbf{x}_i) - \mathbb{E}_{\mathcal{D}}[f(\mathbf{x}_i; \hat{\theta}_{\mathcal{D}})])^2 + \mathbb{E}_{\mathcal{D}}[\{f(\mathbf{x}_i; \hat{\theta}_{\mathcal{D}}) - \mathbb{E}[f(\mathbf{x}_i; \hat{\theta}_{\mathcal{D}})]\}^2]
\end{aligned}$$

Putting these two equation together leads to the expected generalization error:

$$\begin{aligned}
\mathbb{E}_{\mathcal{D},\epsilon}[\mathcal{C}(\mathbf{y}, f(\mathbf{X}; \hat{\theta}_{\mathcal{D}}))] &= \sum_i (f(\mathbf{x}_i) - \mathbb{E}_{\mathcal{D}}[f(\mathbf{x}_i; \hat{\theta}_{\mathcal{D}})])^2 \\
&\quad + \sum_i \mathbb{E}_{\mathcal{D}}[\{f(\mathbf{x}_i; \hat{\theta}_{\mathcal{D}}) - \mathbb{E}[f(\mathbf{x}_i; \hat{\theta}_{\mathcal{D}})]\}^2] \\
&\quad + \sum_i \sigma_\epsilon^2
\end{aligned}$$

Acronyms

ALICE A Large Ion Collider Experiment

ATLAS A Toroidal LHC ApparatuS

BEH Brout-Englert-Higgs

CART Classification and Regression Trees

CCDY charged current Drell-Yan

CERN European Organization for Nuclear Research (EN)

CKS Cohen Kappa Score

CLIC Compact Linear Collider

CM center-of-mass

CMS Compact Muon Solenoid

DIS Deep Inelastic Scattering

DT Decision Tree

ECal electromagnetic calorimeter

EF Event filter

EWT electroweak theory

FCC Future Circular Collider

FFNN Feed-Forward Neural Network

GBDT Gradient Boosting Decision Tree

GWS Glashow-Weinberg-Salam

HCal hadronic calorimeter

HLT High Level Trigger

ID inner detector

LEP Large Electron-Positron Collider

LGBM Light Gradient Boosting Machine

LH left-handed

LHC Large Hadron Collider

LHCb LHC-beauty

LR Logistic Regression

LRSM Left-Right Symmetric Model

LSP lightest Supersymmetric particle

MET missing transverse momentum

ML machine learning

MLE Maximum Likelihood Estimation

MLP Multi-Layer Perceptron

MS muon spectrometer

MSSM Minimal Supersymmetric Standard Model

OLS Ordinary Least Squares

OvO one-vs-one

OvR one-vs-rest

PCA Principal Component Analysis

PDF parton distribution function

PMNS Pontecorvo-Maki-Nakagawa-Sakata

QCD quantum chromodynamics

QED quantum electrodynamics

QFD quantum flavordynamics

QFT quantum field theory

ReLU Rectified Linear Unit

RF radio frequency

RH right-handed

RnF Random Forest

ROI region of interest

SCT Semiconductor Tracker

SM Standard Model

SNO Sudbury Neutrino Observatories

SPS Super Proton Synchrotron

SUSY Supersymmetry

SVM Support Vector Machine

TDAQ The ATLAS Trigger and Data Acquisition system

TRT Transition Radiation Tracker

VEV vacuum expectation value

WIMP weakly interacting massive particle

XGBoost Extreme Gradient Boosting

Bibliography

[1] Georges Aad, Tatevik Abajyan, B Abbott, J Abdallah, S Abdel Khalek, Ahmed Ali Abdelalim, R Aben, B Abi, M Abolins, OS AbouZeid, et al. Observation of a new particle in the search for the standard model higgs boson with the atlas detector at the lhc. *Physics Letters B*, 716(1):1–29, 2012.

[2] Serguei Chatrchyan, Vardan Khachatryan, Albert M Sirunyan, Armen Tumasyan, Wolfgang Adam, Ernest Aguilo, Thomas Bergauer, M Dragicevic, J Erö, C Fabjan, et al. Observation of a new boson at a mass of 125 gev with the cms experiment at the lhc. *Physics Letters B*, 716(1): 30–61, 2012.

[3] Arindam Das, Natsumi Nagata, and Nobuchika Okada. Testing the 2-TeV resonance with trileptons. *Journal of High Energy Physics*, 2016 (3):49, 2016.

[4] Silvia Pascoli, Richard Ruiz, and Cedric Weiland. Heavy neutrinos with dynamic jet vetoes: multilepton searches at $\sqrt{s}$= 14, 27, and 100 TeV. *Journal of High Energy Physics*, 2019(6):49, 2019.

[5] Mark Thomson. *"Modern particle physics*. Cambridge University Press, 2013.

[6] Glenn Elert. The physics hypertextbook, 1998-2020. URL https://physics.info/standard/.

[7] *Why is the Higgs discovery so significant?* Science and Technology Facilities Council, 2017. URL https://stfc.ukri.org/research/particle-physics-and-particle-astrophysics/peter-higgs-a-truly-british-scientist/why-is-the-higgs-discovery-so-significant/.

[8] Benjamin P Abbott, Richard Abbott, TD Abbott, MR Abernathy, Fausto Acernese, Kendall Ackley, Carl Adams, Thomas Adams, Paolo

Addesso, RX Adhikari, et al. Observation of gravitational waves from a binary black hole merger. *Physical review letters*, 116(6):061102, 2016.

[9] Michela Massimi. *Pauli's Exclusion Principle*. Cambridge University Press, 2005. ISBN 0-521-83911-4.

[10] Y Fukuda, T Hayakawa, E Ichihara, K Inoue, K Ishihara, Hirokazu Ishino, Y Itow, T Kajita, J Kameda, S Kasuga, et al. Evidence for oscillation of atmospheric neutrinos. *Physical Review Letters*, 81(8): 1562, 1998.

[11] Elizabeth Gibney and Davide Castelvecchi. Neutrino flip wins physics prize, 2015.

[12] Alan Kostelecky. The status of cpt. *arXiv preprint hep-ph/9810365*, 1998.

[13] Franz Mandl and Graham Shaw. *Quantum field theory*. John Wiley & Sons, 2010.

[14] M. Bellac. Quantum and statistical field theory. 1991.

[15] Richard P Feynman. The principle of least action in quantum mechanics. In *Feynman's Thesis—A New Approach To Quantum Theory*, pages 1–69. World Scientific, 2005. doi: https://doi.org/10.1142/9789812567635_0001.

[16] Gerhard Ecker. Quantum chromodynamics. *arXiv preprint hep-ph/0604165*, 2006.

[17] C. N. Yang and R. L. Mills. Conservation of isotopic spin and isotopic gauge invariance. *Phys. Rev.*, 96:191–195, Oct 1954. doi: 10.1103/PhysRev.96.191. URL https://link.aps.org/doi/10.1103/PhysRev.96.191.

[18] Richard Phillips Feynman. *QED: The strange theory of light and matter*. Princeton University Press, 2006.

[19] Guido Altarelli. The standard electroweak theory and beyond. *arXiv preprint hep-ph/9811456*, pages 27–93, 2000.

[20] Sheldon L Glashow. Partial-symmetries of weak interactions. *Nuclear physics*, 22(4):579–588, 1961. doi: https://doi.org/10.1016/0029-5582(61)90469-2.

[21] Steven Weinberg. A model of leptons. *Physical review letters*, 19(21): 1264, 1967. doi: https://doi.org/10.1103/PhysRevLett.19.1264.

[22] A Salam. N. svartholm, ed. elementary particle physics: Relativistic groups and analyticity. In *Eighth Nobel Symposium. Stockholm: Almquvist and Wiksell*, page 367, 1968.

[23] *Press release: The Nobel Prize in Physics 1979*. Nobel Media AB 2020, 1979. URL https://www.nobelprize.org/prizes/physics/1979/press-release/.

[24] Abdus Salam and Steven Weinberg. Nobel Prize for Physics, 1979. *CERN Courier*, page 395, 1979.

[25] Jeffrey Goldstone. Field theories with «superconductor» solutions. *Il Nuovo Cimento (1955-1965)*, 19(1):154–164, 1961. doi: 10.1007/BF02812722.

[26] Howard Baer and Xerxes Tata. *Weak scale supersymmetry: From superfields to scattering events*. Cambridge University Press, 2006.

[27] STEPHEN P. MARTIN. A supersymmetry primer. *Advanced Series on Directions in High Energy Physics*, page 1–98, Jul 1998. ISSN 1793-1339. doi: 10.1142/9789812839657_0001. URL http://dx.doi.org/10.1142/9789812839657_0001.

[28] Rabindra N Mohapatra. Seesaw mechanism and its implications. In *SEESAW 25*, pages 29–44. World Scientific, 2005.

[29] Darwin Chang and Otto CW Kong. Pseudo-dirac neutrinos. *Physics Letters B*, 477(4):416–423, 2000.

[30] KRS Balaji, Anna Kalliomäki, and Jukka Maalampi. Revisiting pseudo-dirac neutrinos. *Physics Letters B*, 524(1-2):153–160, 2002.

[31] R. N. Mohapatra and J. C. Pati. "natural" left-right symmetry. *Phys. Rev. D*, 11:2558–2561, May 1975. doi: 10.1103/PhysRevD.11.2558. URL https://link.aps.org/doi/10.1103/PhysRevD.11.2558.

[32] Jogesh C. Pati and Abdus Salam. Lepton number as the fourth "color". *Phys. Rev. D*, 10:275–289, Jul 1974. doi: 10.1103/PhysRevD.10.275. URL https://link.aps.org/doi/10.1103/PhysRevD.10.275.

[33] Rabindra N. Mohapatra and Jogesh C. Pati. Left-right gauge symmetry and an "isoconjugate" model of CP violation. *Phys. Rev. D*, 11:566–571, Feb 1975. doi: 10.1103/PhysRevD.11.566. URL https://link.aps.org/doi/10.1103/PhysRevD.11.566.

[34] G. Senjanovic and R. N. Mohapatra. Exact left-right symmetry and spontaneous violation of parity. *Phys. Rev. D*, 12:1502–1505, Sep 1975. doi: 10.1103/PhysRevD.12.1502. URL https://link.aps.org/doi/10.1103/PhysRevD.12.1502.

[35] PS Bhupal Dev, Rabindra N Mohapatra, Werner Rodejohann, and Xun-Jie Xu. Vacuum structure of the left-right symmetric model. *Journal of High Energy Physics*, 2019(2):154, 2019.

[36] Eirik Gramstad. Searches for Supersymmetry in di-Lepton Final States with the ATLAS Detector at $\sqrt{s}$= 7 TeV. 2013.

[37] Richard D Field. The underlying event in hard scattering processes. *arXiv preprint hep-ph/0201192*, 2002.

[38] About CERN. CERN, (10.12.20). URL https://home.cern/about.

[39] Stephanie Sammartino McPherson. *Tim Berners-Lee: Inventor of the World Wide Web*. Twenty-First Century Books, 2009.

[40] Esma Mobs. The CERN accelerator complex - 2019. Complexe des accélérateurs du CERN - 2019. Jul 2019. URL https://cds.cern.ch/record/2684277. General Photo.

[41] XinChou Lou. The Circular Electron Positron Collider. *Nat. Rhev. Phys.*, 1:232–234, 2019. doi: https://doi.org/10.1038/s42254-019-0047-1.

[42] Jie Gao. China's bid for a circular electron-positron collider. *CERN Courier*, 2018.

[43] Shinichiro Michizono. The International Linear Collider. *Nat. Rhev. Phys.*, 1:244–245, 2019. doi: https://doi.org/10.1038/s42254-019-0044-4.

[44] Philip Bambade, Tim Barklow, Ties Behnke, Mikael Berggren, James Brau, Philip Burrows, Dmitri Denisov, Angeles Faus-Golfe, Brian Foster, Keisuke Fujii, et al. The international linear collider: a global project. *arXiv preprint arXiv:1903.01629*, 2019.

[45] The Large Hadron Collider. CERN, (11.12.20). URL https://home.cern/science/accelerators/large-hadron-collider.

[46] Accelerators. CERN, (11.12.20). URL https://home.cern/science/accelerators.

[47] Experiments: LHC experiments. CERN, (11.12.20). URL https://home.cern/science/experiments.

[48] A Airapetian, V Dodonov, L Micu, D Axen, V Vinogradov, D Akerman, B Szeless, P Chochula, C Geich-Gimbel, P Schacht, et al. *ATLAS detector and physics performance: Technical Design Report, 1*, volume 1. 1999.

[49] ATLAS Collaboration. Measurement of the Inelastic Proton-Proton Cross Section at $\sqrt{s}$=13 TeV with the ATLAS Detector at the LHC. *Phys. Rev. Lett.*, 117:182002, Oct 2016. doi: 10.1103/PhysRevLett.117.182002. URL https://link.aps.org/doi/10.1103/PhysRevLett.117.182002.

[50] Computer generated image of the whole ATLAS detector. CERN Document Server, (01.01.21). URL https://cds.cern.ch/record/1095924?ln=en.

[51] How ATLAS detects particles: diagram of particle paths in the detector . CERN Document Server, (01.01.21). URL https://cds.cern.ch/record/1505342?ln=en.

[52] ATLAS Collaboration, Georges Aad, JM Butterworth, J Thion, U Bratzler, PN Ratoff, RB Nickerson, JM Seixas, I Grabowska-Bold, F Meisel, S Lokwitz, et al. The atlas experiment at the cern large hadron collider. *Jinst*, 3:S08003, 2008.

[53] CERN. Overall detector concept. *ATLAS Technical Proposal*, 1994.

[54] DA Scannicchio. Atlas trigger and data acquisition: Capabilities and commissioning. *Nuclear Instruments and Methods in Physics Research Section A: Accelerators, Spectrometers, Detectors and Associated Equipment*, 617(1-3):306–309, 2010.

[55] CMS Collaboration, Vardan Khachatryan, Albert M Sirunyan, Armen Tumasyan, Wolfgang Adam, Thomas Bergauer, Marko Dragicevic, Janos Erö, Christian Fabjan, Markus Friedl, Rudolf Fruehwirth,

et al. Search for heavy neutrinos and W bosons with right-handed couplings in proton-proton collisions at $\sqrt{s}$= 8TeV. *The European Physical Journal C*, 74(11):3149, 2014. doi: https://doi.org/10.1140/epjc/s10052-014-3149-z.

[56] Ian Goodfellow, Yoshua Bengio, and Aaron Courville. *Deep Learning*. MIT Press, 2016. http://www.deeplearningbook.org.

[57] Trevor Hastie, Robert Tibshirani, and Jerome Friedman. *The elements of statistical learning: data mining, inference, and prediction*. Springer Science & Business Media, 2009.

[58] Pankaj Mehta, Marin Bukov, Ching-Hao Wang, Alexandre GR Day, Clint Richardson, Charles K Fisher, and David J Schwab. A high-bias, low-variance introduction to machine learning for physicists. *Physics reports*, 810:1–124, 2019.

[59] Jose Manuel Pereira, Mario Basto, and Amelia Ferreira da Silva. The logistic lasso and ridge regression in predicting corporate failure. *Procedia Economics and Finance*, 39:634–641, 2016.

[60] William S Noble. What is a support vector machine? *Nature biotechnology*, 24(12):1565–1567, 2006.

[61] Dennis W Ruck, Steven K Rogers, and Matthew Kabrisky. Feature selection using a multilayer perceptron. *Journal of Neural Network Computing*, 2(2):40–48, 1990.

[62] Sandra Vieira, Walter HL Pinaya, and Andrea Mechelli. Using deep learning to investigate the neuroimaging correlates of psychiatric and neurological disorders: Methods and applications. *Neuroscience & Biobehavioral Reviews*, 74:58–75, 2017.

[63] Diederik P Kingma and Jimmy Ba. Adam: A method for stochastic optimization. *arXiv preprint arXiv:1412.6980*, 2014.

[64] S Rasoul Safavian and David Landgrebe. A survey of decision tree classifier methodology. *IEEE transactions on systems, man, and cybernetics*, 21(3):660–674, 1991.

[65] Svante Wold, Kim Esbensen, and Paul Geladi. Principal component analysis. *Chemometrics and intelligent laboratory systems*, 2(1-3):37–52, 1987.

[66] J Ross Quinlan et al. Bagging, boosting, and c4. 5. In *Aaai/iaai, Vol. 1*, pages 725–730, 1996.

[67] Leo Breiman. Random forests. *Machine learning*, 45(1):5–32, 2001.

[68] Gunnar Rätsch, Takashi Onoda, and K-R Müller. Soft margins for adaboost. *Machine learning*, 42(3):287–320, 2001.

[69] Jerome H Friedman. Stochastic gradient boosting. *Computational statistics & data analysis*, 38(4):367–378, 2002.

[70] Guolin Ke, Qi Meng, Thomas Finley, Taifeng Wang, Wei Chen, Weidong Ma, Qiwei Ye, and Tie-Yan Liu. Lightgbm: A highly efficient gradient boosting decision tree. *Advances in neural information processing systems*, 30:3146–3154, 2017.

[71] Tianqi Chen and Carlos Guestrin. Xgboost: A scalable tree boosting system. In *Proceedings of the 22nd acm sigkdd international conference on knowledge discovery and data mining*, pages 785–794, 2016.

[72] Dymitr Ruta and Bogdan Gabrys. Classifier selection for majority voting. *Information fusion*, 6(1):63–81, 2005.

[73] Jingjing Cao, Sam Kwong, Ran Wang, Xiaodong Li, Ke Li, and Xiangfei Kong. Class-specific soft voting based multiple extreme learning machines ensemble. *Neurocomputing*, 149:275–284, 2015.

[74] Mary L McHugh. Interrater reliability: the kappa statistic. *Biochemia medica*, 22(3):276–282, 2012.

[75] F. Pedregosa, G. Varoquaux, A. Gramfort, V. Michel, B. Thirion, O. Grisel, M. Blondel, P. Prettenhofer, R. Weiss, V. Dubourg, J. Vanderplas, A. Passos, D. Cournapeau, M. Brucher, M. Perrot, and E. Duchesnay. Scikit-learn: Machine learning in Python. *Journal of Machine Learning Research*, 12:2825–2830, 2011.